

Programming the magnitude and persistence of antibody responses with innate immunity

Sudhir Pai Kasturi^{1,2}, Ioanna Skountzou^{1,3}, Randy A. Albrecht⁴, Dimitrios Koutsonanos³, Tang Hua^{1,2}, Helder I. Nakaya^{1,2}, Rajesh Ravindran^{1,2}, Shelley Stewart⁵, Munir Alam⁵, Marcin Kwissa^{1,2}, Francois Villinger^{1,2,6}, Niren Murthy⁷, John Steel⁴, Joshy Jacob^{1,2,3}, Robert J. Hogan⁸, Adolfo García-Sastre^{4,9,10}, Richard Compans^{1,3} & Bali Pulendran^{1,2,6}

Many successful vaccines induce persistent antibody responses that can last a lifetime. The mechanisms by which they do so remain unclear, but emerging evidence indicates that they activate dendritic cells via Toll-like receptors (TLRs)^{1,2}. For example, the yellow fever vaccine YF-17D, one of the most successful empiric vaccines ever developed³, activates dendritic cells via multiple TLRs to stimulate proinflammatory cytokines^{4,5}. Triggering specific combinations of TLRs in dendritic cells can induce synergistic production of cytokines⁶, which results in enhanced T-cell responses, but its impact on antibody responses remain unknown. Learning the critical parameters of innate immunity that program such antibody responses remains a major challenge in vaccinology. Here we demonstrate that immunization of mice with synthetic nanoparticles containing antigens plus ligands that signal through TLR4 and TLR7 induces synergistic increases in antigen-specific, neutralizing antibodies compared to immunization with nanoparticles containing antigens plus a single TLR ligand. Consistent with this there was enhanced persistence of germinal centres and of plasma-cell responses, which persisted in the lymph nodes for >1.5 years. Surprisingly, there was no enhancement of the early short-lived plasma-cell response relative to that observed with single TLR ligands. Molecular profiling of activated B cells, isolated 7 days after immunization, indicated that there was early programming towards B-cell memory. Antibody responses were dependent on direct triggering of both TLRs on B cells and dendritic cells, as well as on T-cell help. Immunization protected completely against lethal avian and swine influenza virus strains in mice, and induced robust immunity against pandemic H1N1 influenza in rhesus macaques.

We designed a nanoparticle-based vaccine, similar to a virus in size and composition. A biodegradable synthetic polymer, poly(D,L-lactico-glycolic acid) (PLGA)⁷, was used to synthesize ~300-nM-sized nanoparticles containing the TLR ligands MPL (TLR4 ligand), R837 (TLR7 ligand), or both ligands, together with an antigen (Supplementary Fig. 1). Immunization of mice with nanoparticles containing MPL and R837 (PLGA(MPL+R837)) plus antigen induced enhanced antibody and T-cell responses, compared to immunization with soluble antigen plus MPL and R837 (data not shown). Consistent with recent observations^{8,9}, delivery of antigen and TLR ligands in separate nanoparticles induced a stronger antibody response than delivery of both in the same nanoparticle (Supplementary Fig. 2). Initially, cohorts of C57BL/6 mice were immunized with nanoparticles containing chicken ovalbumin (OVA) alone (PLGA(OVA)), or (PLGA(OVA)) together with PLGA(MPL), PLGA(R837), or (PLGA(MPL+R837)). OVA emulsified in alum was used as a control. Immunization with PLGA(MPL) or PLGA(R837) plus nanoparticles containing 50 µg or 10 µg of OVA (Supplementary Figs 3a, 4a), induced enhanced

OVA-specific antibody titres after immunization. Notably, there was a synergistic enhancement of the antibody titres in mice that received PLGA(MPL+R837) (Supplementary Figs 3a, 4a). Secondary immunization with the same immunogen 5 weeks later markedly increased titres in all groups, with the synergy effect with PLGA(MPL+R837) still evident, especially at the lower 10 µg dose (Supplementary Figs 3b, 4b). Thus, in all following experiments we used 10 µg of antigen. In addition to OVA, we also used other antigens including the protective antigen (PA) from *Bacillus anthracis*¹⁰ (Supplementary Fig. 5), and haemagglutinin (HA) from avian influenza H5N1 virus¹¹ (Fig. 1). As observed with OVA, there was a synergistic enhancement in the antigen-specific antibody responses after primary and secondary immunization of mice with PLGA(MPL+R837) plus PLGA(PA) (Supplementary Fig. 5a, b), or PLGA(HA) (Fig. 1a, b).

The avidity of antigen-antibody binding is one index of the quality of the antibody response¹². We used a surface plasmon resonance (SPR) assay to assess avidity. Sera from mice immunized with PLGA(MPL+R837) plus PLGA(HA) gave the highest binding response (Fig. 1c). The slower dissociation and higher association rates indicate that immunization with PLGA(MPL+R837) plus PLGA(HA) induced a more enhanced high-affinity antibody response than that induced by PLGA(MPL) or PLGA(R837) plus PLGA(HA). A similar trend was also observed with PA as an antigen (Supplementary Fig. 5c). Consistent with the effects on enzyme-linked immunosorbent assay (ELISA) titres and avidity, mice immunized with PLGA(MPL+R837) plus PLGA(HA) had the greatest neutralization antibody titres (Fig. 1d).

Next we assessed the mechanism by which PLGA(MPL+R837) induced synergistic responses. PLGA(MPL+R837) enhanced the secretion of proinflammatory cytokines by dendritic cells *in vitro*, compared to PLGA(MPL) or PLGA(R837) (Supplementary Fig. 6a). Further, *in vivo* depletion of dendritic cells in CD11c-DTR transgenic mice¹³, or Langerhans cells using the Langerin-DTR mice¹⁴, resulted in diminished antibody titres (Supplementary Fig. 6b, c). These data demonstrate a critical role for dendritic cells in mediating the antibody response to immunization with PLGA(MPL+R837). Signalling via TLR4 and TLR7 is dependent on the adaptor proteins MyD88 or TRIF (also known as TICAM-1); MPL is reported to signal predominantly via TRIF¹⁵. Both MyD88 and TRIF were required for antibody responses stimulated by PLGA(MPL+R837) plus PLGA(OVA) (Supplementary Fig. 7).

B cells express and respond to TLRs^{16,17}. Thus, we determined whether direct triggering of TLRs on B cells was essential for antibody responses. *In vitro* stimulation of naive splenic B cells with PLGA(MPL+R837) synergistically enhanced B-cell proliferation relative to stimulation with PLGA(MPL) or PLGA(R837) (data not shown). To assess this

¹Emory Vaccine Center, Emory University, Atlanta, Georgia 30329, USA. ²Yerkes National Primate Research Center, Emory University, Atlanta, Georgia 30329, USA. ³Department of Microbiology and Immunology, Emory University, Atlanta, Georgia 30322, USA. ⁴Department of Microbiology, Mount Sinai School of Medicine, New York, New York 10029, USA. ⁵Duke Human Vaccine Institute, Duke University Medical Center, Durham, North Carolina 103020, USA. ⁶Department of Pathology, Emory University School of Medicine, Atlanta, Georgia 30322, USA. ⁷The Wallace H. Coulter Department of Biomedical Engineering, Georgia Institute of Technology, Atlanta, Georgia 30332, USA. ⁸Department of Anatomy and Radiology, College of Veterinary Medicine, University of Georgia, Athens, Georgia 30602, USA. ⁹Department of Medicine, Division of Infectious Diseases, Mount Sinai School of Medicine, New York, New York 10029, USA. ¹⁰Global Health and Emerging Pathogens Institute, Mount Sinai School of Medicine, New York, New York 10029, USA.

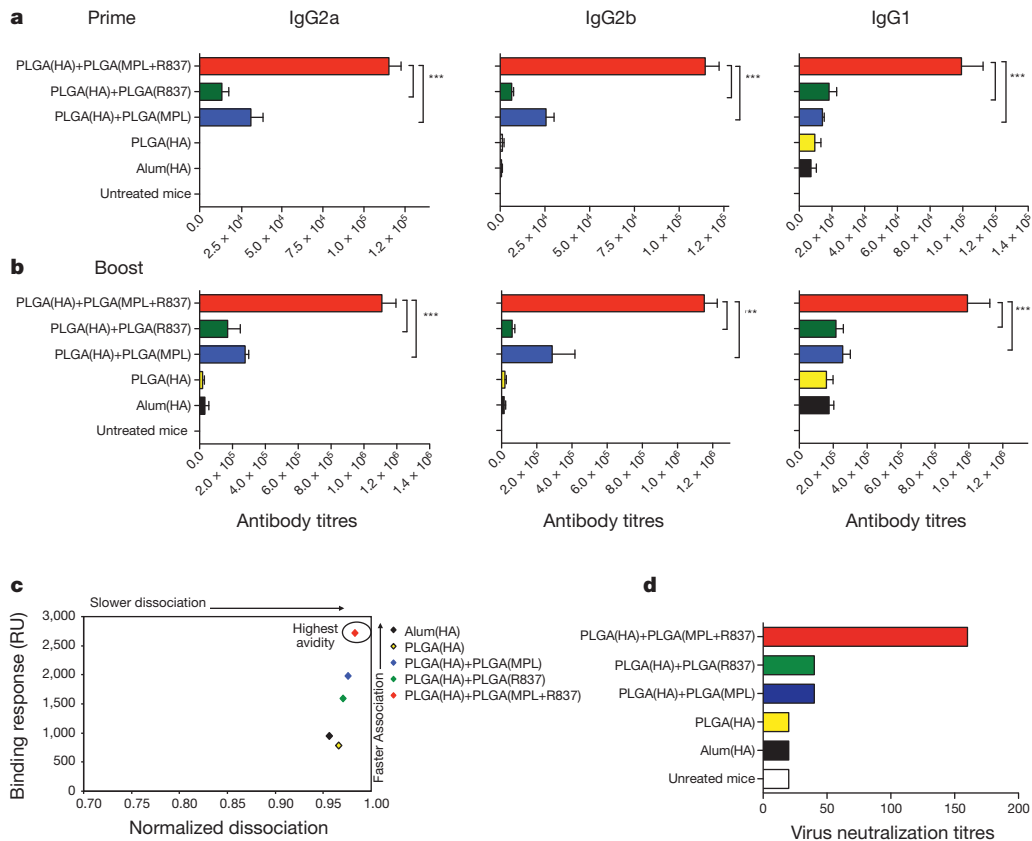


Figure 1 | Combination of MPL and R837 in PLGA nanoparticles mediates synergistic enhancement of antibody responses against H5N1-influenza-derived HA. **a, b**, Antibody titres at 4 weeks after primary and secondary immunization (mean + s.e.m. of four independent experiments, with 4–5 mice per treatment group in each experiment) are shown for IgG2a, IgG2b and IgG1 isotypes. *** $P < 0.001$, ** $P < 0.01$ (one-way ANOVA with Bonferroni post-hoc test). **c**, Pooled serum samples from HA-immunized mice at day 28 after

secondary immunization boost immunization were tested for their HA-binding avidity using BIAcore SPR-based protein binding assay. Data are representative of plots from one of two independent experiments. RU, maximal response unit. **d**, Virus neutralization assays were performed with pooled serum samples from treatment groups assayed in duplicates. Results shown are representative titres from one of two independent experiments.

effect *in vivo*, mice lacking B cells (μ MT mice) were reconstituted with B cells from wild-type mice, or $MyD88^{-/-}$ or $Trif^{-/-}$ mice, and then immunized with PLGA(MPL+R837) plus PLGA(OVA) (Fig. 2a). In μ MT mice reconstituted with wild-type B cells immunization induced a synergistic enhancement of antibody responses (Fig. 2b). However, μ MT mice reconstituted with $MyD88^{-/-}$ or $Trif^{-/-}$ B cells had diminished antibody titres (Fig. 2c), demonstrating that direct TLR triggering on B cells was required for stimulation of antibody responses. We determined then whether the synergy was dependent on co-expression of TLR4 and TLR7 on the same B cell, or whether there could be complementation between B cells lacking different TLRs. We thus transferred B cells from $Tlr4^{-/-}$ mice, or $Tlr7^{-/-}$ mice, or a 1:1 mixture of B cells from $Tlr4^{-/-}$ and $Tlr7^{-/-}$ mice into μ MT mice. Immunization with PLGA(MPL+R837) and PLGA(OVA) demonstrated a requirement for co-expression of both TLRs on the same B cell (Fig. 2d).

Lastly, TLR activation of dendritic cells is known to stimulate antigen-specific $CD4^{+}$ T-helper cells, which are essential for induction of antibody responses¹⁸. Depletion of $CD4^{+}$ T-helper cells before immunization diminished antibody responses (Supplementary Fig. 8). Consistent with this, immunization with PLGA(MPL+R837) and PLGA(OVA) resulted in an enhanced antigen-specific $CD4^{+}$ T-cell response (Fig. 2e). Interestingly, we observed (Fig. 2f) that OVA-specific $CD4^{+}$ T-helper cell responses were substantially reduced in μ MT mice transferred with $MyD88^{-/-}$ or $Trif^{-/-}$ B cells (in which the antibody responses were severely compromised; Fig. 2c), indicating a requirement for activated B cells in mediating enhanced activation of $CD4^{+}$ T-helper cells, as demonstrated previously¹⁹.

Antibody responses develop along two anatomically and functionally distinct pathways²⁰. The extrafollicular pathway rapidly generates short-lived, antibody-producing cells (plasma cells), and the germinal-centre pathway generates memory B cells and long-lived plasma cells that secrete high-affinity antibody²⁰. We determined whether immunization with nanoparticles containing different adjuvants differentially regulated the two pathways. Thus, mice immunized with the different adjuvants were killed at day 7, lymph nodes isolated and the presence of antibody-producing plasma cells evaluated by immunohistology. There was no apparent difference in the IgG^{+} plasma cells, at day 7, between mice immunized with various adjuvants (Supplementary Fig. 9). We investigated also the kinetics of germinal-centre formation following immunization. Notably, mice immunized with both TLR ligands had a greatly enhanced and sustained germinal-centre response compared to those immunized with a single TLR ligand, (Fig. 3a, b and Supplementary Fig. 9). At day 28 there were approximately 10–12 germinal centres per lymph node and at day 42 there were about 6 germinal centres per lymph node, significantly higher than the numbers observed in lymph nodes of mice immunized with single TLR ligands (Fig. 3a, b). By 8 weeks after immunization the numbers of germinal centres were still substantially higher in the PLGA(MPL+R837) group than in the other groups (Fig. 3b). This demonstrates that PLGA(MPL+R837) preferentially enhances the germinal-centre pathway.

Further, assessment of antigen-specific IgG-secreting plasma cells by the enzyme-linked immunosorbent spot (ELISPOT) assay, indicated no differences in the numbers of plasma cells at day 7 in the

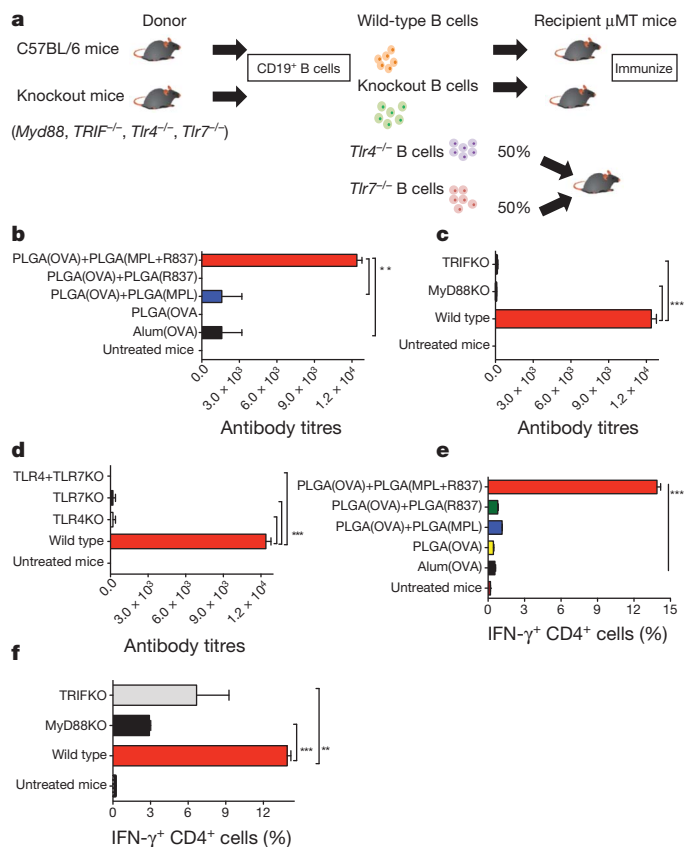


Figure 2 | Synergistic enhancement of antibody responses is dependent on the presence of TLRs on B cells. **a**, B-cell-deficient mice (μ MT mice) were reconstituted with 40×10^6 B cells from C57BL/6 mice or from *MyD88*^{-/-}, *Trif*^{-/-}, *Tlr4*^{-/-} or *Tlr7*^{-/-} mice, or equal numbers of *Tlr4*^{-/-} and *Tlr7*^{-/-} deficient cells to determine whether expression of TLRs and co-expression of TLR4 and TLR7 on the same B cell was necessary for enhancement of antibody responses. Mice were immunized with 10 μ g of OVA encapsulated in PLGA nanoparticles and adjuvants. **b–d**, Mice were bled at day 28 after primary immunization and OVA-specific total IgG antibody responses were determined using ELISA. Antibody titres are shown (mean \pm s.e.m. of two independent experiments, with 3 mice per treatment group in each experiment). KO, knockout. *** $P < 0.001$, ** $P < 0.01$ (one-way ANOVA with Bonferroni post-hoc test). **e**, The magnitude of OVA-specific IFN- γ -producing memory CD4⁺ T cells in the draining lymph nodes of μ MT mice is shown with representative FACS plots. **f**, The magnitude of OVA-specific IFN- γ -producing memory CD4⁺ T cells in the draining lymph nodes is dependent on MyD88 and TRIF expression on B cells. Graphs represent mean frequencies \pm s.d. of triplicate cultures of pooled lymph node cells from one out of two independent experiments.

MPL alone versus MPL+R837 groups (Fig. 3c). At day 28 there were enhanced numbers of plasma cells in the PLGA(MPL+R837) group relative to single TLR-ligand groups. Secondary immunization with the same antigen plus adjuvant resulted in a profoundly enhanced and sustained memory response in the PLGA(MPL+R847) group (Fig. 3c). Notably, there was a persistent plasma-cell response in the lymph node for >1.5 years. Interestingly, there was no corresponding enhancement in the numbers of antigen-specific plasma cells in the bone marrow—a known destination for plasma cells²¹—in the PLGA(MPL+R837) group relative to the single TLR-ligand groups (data not shown). This demonstrates that immunization with PLGA(MPL+R837) preferentially enhances memory B-cell generation. Consistent with this, fluorescence-activated cells sorting (FACS) analysis²² revealed enhanced numbers of isotype-switched, antigen-specific B cells in the PLGA(MPL+R837) group relative to the PLGA(MPL) or PLGA(R837) groups during the memory phase after a secondary boost, but no such enhancement early during the primary response (Supplementary Fig. 10).

The effects of PLGA(MPL+R837) on the germinal-centre pathway might have occurred via early programming of antigen-specific B cells, or as a result of the continued presence of antigen and/or adjuvant. To determine whether there was any early programming of B cells, we isolated isotype-switched, antigen-experienced B cells by FACS at 7 days after immunization with nanoparticles containing various adjuvants plus OVA, and performed microarray analyses to assess their molecular signatures. Notably, there was a great enrichment for genes normally expressed in memory B cells²³, in the cells isolated from mice immunized with PLGA(MPL+R837) plus PLGA(OVA); in contrast, in cells isolated from mice immunized with either PLGA(MPL) or PLGA(R837) plus PLGA(OVA), there was no such enrichment (Supplementary Fig. 11a–c). Such genes included *Bcl2*, *Bcl11a*, *Tank*, several type-I interferon (IFN)-related genes, *Plcg2* and *Cd38*, which are known to have key roles in memory B-cell formation, and several genes that regulate the survival, proliferation and differentiation of germinal-centre B cells, such as *Il17ra*, *Il18r1*, *Pax5*, *Ifngr2*, *Bcor* and *Irf1* (Supplementary Fig. 11a, b). These data indicate that immunization with antigen and MPL+R837 stimulates early programming to the germinal-centre/memory pathway.

Next we determined whether immunization also enhanced antigen-specific memory T-cell responses. There was a synergistic enhancement of OVA-specific IFN- γ -producing CD4⁺ T-helper cell responses at 8 weeks after secondary immunization (Supplementary Fig. 12a, b), but not at days 7 or 14 after primary immunization (data not shown), indicating a preferential effect on the generation of memory T cells. Similar results were observed in mice immunized with HA and PA antigen, even 1.5 years after immunization (Supplementary Fig. 12c–f). PLGA(MPL+R837) immunization also enhanced the antigen-specific CD8⁺ T-cell responses. Although no synergistic enhancement was observed in the frequencies of IFN- γ producing, OVA-specific CD8⁺ T cells at day 7 after primary immunization, there was an increase at day 7 after secondary immunization (Supplementary Fig. 13). Polyfunctional T cells secreting multiple cytokines such as IFN- γ , TNF- α and IL-2 have been implicated in mediating enhanced protection²⁴. We also observed enhanced numbers of triple (IFN- γ , TNF- α and IL-2) and double cytokine (IFN- γ , IL-2) producing CD8⁺ T cells in mice immunized with PLGA(MPL+R837) (Supplementary Fig. 14a, b). Thus, PLGA(MPL+R837) enhances the magnitude and quality of the antigen-specific memory CD4⁺ and CD8⁺ T cells. To assess the relevance of enhanced B- and T-cell responses for protective immunity, we evaluated efficacy of these vaccines in mediating protection in mice, against the 2009 pandemic H1N1 influenza A virus¹¹ (Supplementary Figs 15, 16) and the H5N1 avian influenza virus^{11,25} (Supplementary Fig. 17). In each case, there was enhanced antigen-specific humoral immunity and survival against lethal infection of mice (Supplementary Figs 15–17).

Finally, we assessed the immunogenicity of PLGA(MPL+R837) in non-human primates. In humans and non-human primates, unlike in mice, TLR7 is selectively expressed on plasmacytoid dendritic cells, and not on myeloid dendritic cells². As multiple dendritic-cell subsets seem to be involved in the stimulation of antibody responses by PLGA(MPL+R837) (Supplementary Fig. 6b, c), we used R848, which signals through both TLR7 and TLR8²⁶. Further, in humans, although naive B cells do not express TLRs 4, 7 or 8, activated B cells including plasma cells upregulate and respond to these TLRs²⁷. Current human monovalent vaccines against H1N1 influenza contain 15 μ g of HA (effectively 45 μ g of whole inactivated virus (WIV))²⁸. We therefore used 50 μ g of WIV ($\sim 16 \mu$ g HA), as well as a fivefold lower dose ($\sim 3 \mu$ g HA), with and without adjuvant, to determine whether there was a dose-sparing effect. Four cohorts of four rhesus macaques per cohort were immunized subcutaneously with the indicated doses of WIV, with or without PLGA(MPL+R837) or PLGA(MPL+R848) (Fig. 4a). After a single immunization with 10 μ g or 50 μ g of WIV without any adjuvants, there was no detectable antibody response (Fig. 4b–d). In contrast, adjuvanting with PLGA(MPL+R848)

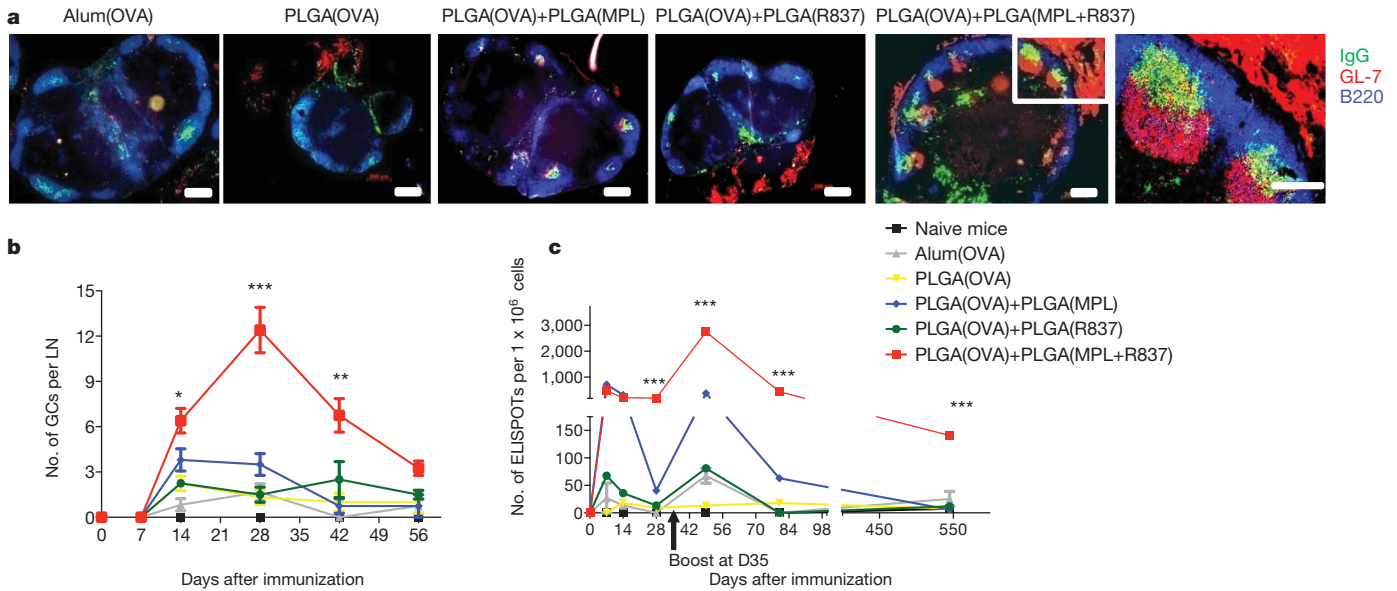


Figure 3 | Immunization with nanoparticles containing MPL and R837 induces persistent germinal centres and long-lived antibody-forming cells in draining lymph nodes. **a**, C57BL/6 mice were immunized with OVA encapsulated in nanoparticles with MPL + R837 plus antigen. Four weeks after primary immunization, draining lymph nodes were excised, tissue sections prepared and stained for germinal centres (GL-7, red; B220, blue; and IgG, green). Images are representative of two independent experiments with draining lymph nodes obtained from 2–3 mice per treatment condition per experiment. Scale bars, 200 μ m for first five panels from left and 100 μ m for

right-hand panel. **b**, Germinal centres (GCs) were counted in lymph node (LN) sections at the time points indicated and represented as mean \pm s.e.m. from 4–6 draining lymph nodes from $n = 2$ –3 mice per treatment group. **c**, ELISPOT assay. Combination of TLR4 and TLR7 ligands has no effect on the short-lived antibody-secreting cells, relative to single TLR ligands, but stimulates long-lived antibody-secreting cells that persist for ~ 1.5 years. Graph represents average spots per 1×10^6 total lymph node cells \pm s.e.m. from duplicate cultures per treatment group. Data are representative of at least 2–3 independent experiments per time point indicated.

induced robust antibody responses, as early as 2 weeks (Fig. 4b–d). Immunization with PLGA(MPL+R837) yielded enhanced binding antibodies, but had more modest effects on HA inhibition and neutralization titres (Fig. 4b–d). Notably, the magnitude of HA inhibition and neutralization titres 28 days after a single immunization with PLGA(MPL+R848) was much greater than 1/40, considered the correlate of protection against influenza in humans (Fig. 4c, d)²⁹. There was at least a fivefold dose-sparing effect, as 10 μ g of antigen plus PLGA(MPL+R848) yielded a much greater response than that

induced by 50 μ g of antigen alone (Fig. 4b–d). Secondary immunizations enhanced the antibody responses in all of the groups, and although PLGA(MPL+R848) still induced the strongest response, PLGA(MPL+R837) also induced responses greater than that required for protection (Fig. 4c, d). Further, the dose-sparing effect was still evident after secondary immunization (Fig. 4b–d).

Here we have described a nanoparticle-based vaccine that resembles a virus in size and composition, and that recapitulates the immunogenicity of live viral vaccines⁵. A notable feature of the immune

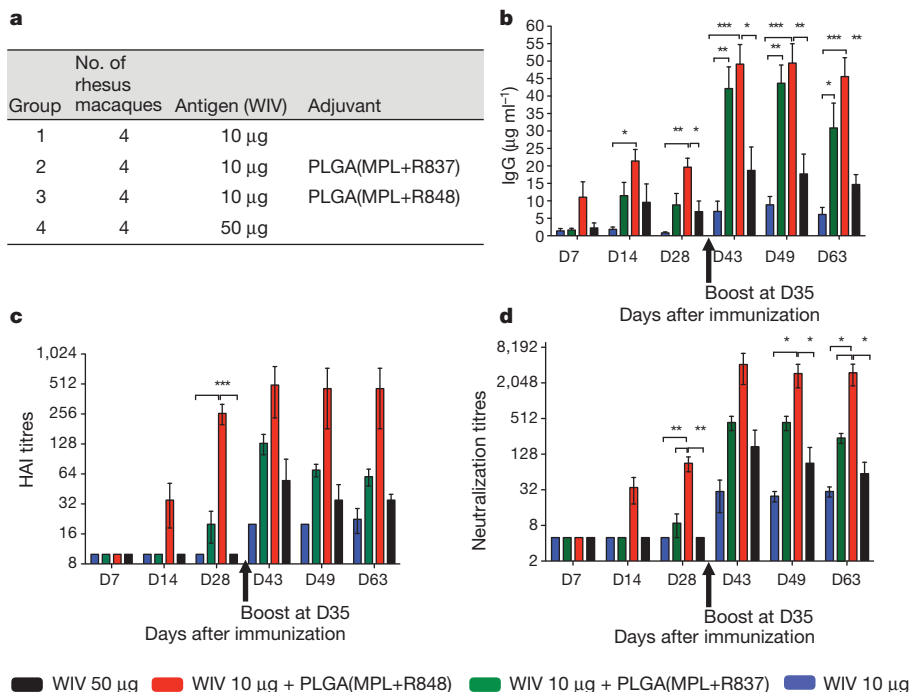


Figure 4 | Immunization of rhesus macaques with 2009 pandemic H1N1 influenza A, whole inactivated virus and nanoparticles containing MPL+R837 or MPL+R848 induces robust humoral immune responses. **a**, Rhesus macaques ($n = 4$) were immunized with 10 μ g of H1N1 WIV with or without nanoparticle-encapsulated MPL+R837 or MPL+R848. Fifty micrograms of MPL and 750 μ g of R837 and R848 encapsulated in nanoparticles were used per macaque. One group of 4 animals was also immunized with 50 μ g of WIV to determine dose-sparing effects mediated by adjuvants. **b**, Antibodies against WIV were analysed as described in Methods and results are represented as mean \pm s.e.m. **c**, HA inhibition (HAI) titres were assayed at indicated time points and are represented as mean \pm s.e.m. **d**, Neutralization titres as represented as the reciprocal of the plasma dilution that decreased the number of plaques formed by the live virus by 50%. Statistical significance was analysed by ANOVA (Bonferroni post-hoc test) and indicated on the figures wherever significant. *** $P < 0.001$, ** $P < 0.01$, * $P < 0.05$. Data are represented as mean \pm s.e.m.

response stimulated by this vaccine is in the induction of long-lived germinal centres and persistent antigen-specific B- and T-cell responses, similar to that seen with viral infections³⁰. Importantly, although all TLR ligands stimulate primary antibody responses, the combined TLR4 and TLR7 stimulus enhances the germinal-centre pathway of memory B-cell formation and long-lived plasma-cell responses, far more efficiently than stimulation with single TLR ligands (Supplementary Fig. 18). The molecular signatures of antigen-activated B cells isolated early after immunization indicates early programming towards a quasi memory state (Supplementary Fig. 11), but it is also likely that persistent antigen/adjuvants, as evidenced by persistent immune complexes in germinal centres (Fig. 3), have a role. A curious aspect of our data is the requirement for the TLR ligands and antigens to be delivered on two separate particles, consistent with other studies^{8,9}. From a practical perspective, this offers flexibility in coupling a generic adjuvant-containing particle with another particle containing antigen from any pathogen. Further, as each of the components of this vaccine (MPL, R837, PLGA) have been licensed for human use, this vaccine formulation may provide a universal platform for vaccine design against pandemics and emerging infections.

METHODS SUMMARY

Synthesis and characterization of nanoparticles. Antigens were encapsulated in PLGA nanoparticles using a water in oil in water (w/o/w) emulsion technique. MPL was encapsulated in PLGA formulations using an oil in water (o/w) single emulsion process as described before with slight modifications⁸. Sizing of the nanoparticles was conducted using a dynamic light scattering, and protein loading was assessed as described before³¹.

Immunization of mice and non-human primates. Eight-to-twelve week old BALB/c or C57BL/6 mice (Charles River) were immunized with 10 µg of antigen encapsulated in nanoparticles suspended in 200 µl of PBS subcutaneously at the base of the tail. Ten-to-thirteen year old female Rhesus Macaques (7–10 kg) were used and were immunized subcutaneously in the right leg. All procedures were performed in accordance with the Emory School of Medicine Institutional Animal Care and Use Committee guidelines.

Antigen-antibody affinity binding analysis. SPR binding measurements were carried out on a BIAcore 3000 instrument (BIAcore/GE Healthcare).

H5N1 microneutralization assays. This was performed as described previously²⁵.

B-cell ELISPOT. 1×10^6 lymph node cells were serially diluted and cultured overnight in duplicate wells of OVA-coated nitrocellulose-lined 96-well plates (Millipore). Cells were discarded and wells were treated with biotinylated goat anti-mouse total IgG (Southern Biotech) in PBS/0.5% Tween-20 plus 1% FBS for 1.5 h at room temperature (25 °C). Wells were washed and treated with streptavidin alkaline phosphatase (Vector Labs) for another 1.5 h at room temperature. Finally, NBT/BCIP colorimetric substrate for alkaline phosphatase was added to the wells and the reaction was stopped after visualization of purple coloured spots.

Affymetrix GeneChip analysis. Total RNA from sorted B cells was purified using Trizol (Invitrogen). All RNA samples were checked for purity and for integrity and amplified, processed through EXON Module, fragmented and labelled. Labelled targets hybridized to GeneChip Mouse Gene 1.0ST arrays (Affymetrix).

Full Methods and any associated references are available in the online version of the paper at www.nature.com/nature.

Received 27 May; accepted 2 December 2010.

- Pulendran, B. & Ahmed, R. Translating innate immunity into immunological memory: implications for vaccine development. *Cell* **124**, 849–863 (2006).
- Kawai, T. & Akira, S. The role of pattern-recognition receptors in innate immunity: update on Toll-like receptors. *Nature Immunol.* **11**, 373–384 (2010).
- Pulendran, B. Learning immunology from the yellow fever vaccine: innate immunity to systems vaccinology. *Nature Rev. Immunol.* **9**, 741–747 (2009).
- Querec, T. *et al.* Yellow fever vaccine YF-17D activates multiple dendritic cell subsets via TLR2, 7, 8, and 9 to stimulate polyvalent immunity. *J. Exp. Med.* **203**, 413–424 (2006).
- Querec, T. D. *et al.* Systems biology approach predicts immunogenicity of the yellow fever vaccine in humans. *Nature Immunol.* **10**, 116–125 (2009).
- Napolitani, G., Rinaldi, A., Bertoni, F., Sallusto, F. & Lanzavecchia, A. Selected Toll-like receptor agonist combinations synergistically trigger a T helper type 1-polarizing program in dendritic cells. *Nature Immunol.* **6**, 769–776 (2005).
- Peek, L. J., Middaugh, C. R. & Berkland, C. Nanotechnology in vaccine delivery. *Adv. Drug Deliv. Rev.* **60**, 915–928 (2008).

- Kazzaz, J. *et al.* Encapsulation of the immune potentiators MPL and RC529 in PLG microparticles enhances their potency. *J. Control. Release* **110**, 566–573 (2006).
- Singh, M., Chakrapani, A. & O'Hagan, D. Nanoparticles and microparticles as vaccine-delivery systems. *Expert Rev. Vaccines* **6**, 797–808 (2007).
- Young, J. A. & Collier, J. R. Attacking anthrax. *Sci. Am.* **286**, 48–59 (2002).
- Chen, G. L. & Subbarao, K. Live attenuated vaccines for pandemic influenza. *Curr. Top. Microbiol. Immunol.* **333**, 109–132 (2009).
- Hengartner, L., Zinkernagel, R. M. & Hengartner, H. Antiviral antibody responses: the two extremes of a wide spectrum. *Nature Rev. Immunol.* **6**, 231–243 (2006).
- Jung, S. *et al.* *In vivo* depletion of CD11c⁺ dendritic cells abrogates priming of CD8⁺ T cells by exogenous cell-associated antigens. *Immunity* **17**, 211–220 (2002).
- Kissenpfennig, A. *et al.* Dynamics and function of Langerhans cells *in vivo*: dermal dendritic cells colonize lymph node areas distinct from slower migrating Langerhans cells. *Immunity* **22**, 643–654 (2005).
- Mata-Haro, V. *et al.* The vaccine adjuvant monophosphoryl lipid A as a TRIF-biased agonist of TLR4. *Science* **316**, 1628–1632 (2007).
- Bernasconi, N. L., Traggiai, E. & Lanzavecchia, A. Maintenance of serological memory by polyclonal activation of human memory B cells. *Science* **298**, 2199–2202 (2002).
- Pasare, C. & Medzhitov, R. Control of B-cell responses by Toll-like receptors. *Nature* **438**, 364–368 (2005).
- Mitchison, N. A. T-cell–B-cell cooperation. *Nature Rev. Immunol.* **4**, 308–312 (2004).
- van Essen, D., Dullforce, P., Brocker, T. & Gray, D. Cellular interactions involved in Th cell memory. *J. Immunol.* **165**, 3640–3646 (2000).
- McHeyzer-Williams, L. J. & McHeyzer-Williams, M. G. Antigen-specific memory B cell development. *Annu. Rev. Immunol.* **23**, 487–513 (2005).
- Slifka, M. K., Antia, R., Whitmire, J. K. & Ahmed, R. Humoral immunity due to long-lived plasma cells. *Immunity* **8**, 363–372 (1998).
- McHeyzer-Williams, M. G., McLean, M. J., Lalor, P. A. & Nossal, G. J. Antigen-driven B cell differentiation *in vivo*. *J. Exp. Med.* **178**, 295–307 (1993).
- Luckey, C. J. *et al.* Memory T and memory B cells share a transcriptional program of self-renewal with long-term hematopoietic stem cells. *Proc. Natl Acad. Sci. USA* **103**, 3304–3309 (2006).
- Wille-Reece, U. *et al.* HIV Gag protein conjugated to a Toll-like receptor 7/8 agonist improves the magnitude and quality of Th1 and CD8⁺ T cell responses in nonhuman primates. *Proc. Natl Acad. Sci. USA* **102**, 15190–15194 (2005).
- Steel, J. *et al.* Live attenuated influenza viruses containing NS1 truncations as vaccine candidates against H5N1 highly pathogenic avian influenza. *J. Virol.* **83**, 1742–1753 (2009).
- Jurk, M. *et al.* Human TLR7 or TLR8 independently confer responsiveness to the antiviral compound R-848. *Nature Immunol.* **3**, 499 (2002).
- Dorner, M. *et al.* Plasma cell toll-like receptor (TLR) expression differs from that of B cells, and plasma cell TLR triggering enhances immunoglobulin production. *Immunology* **128**, 573–579 (2009).
- Clark, T. W. *et al.* Trial of 2009 influenza A (H1N1) monovalent MF59-adjuvanted vaccine. *N. Engl. J. Med.* **361**, 2424–2435 (2009).
- Potter, C. W. & Oxford, J. S. Determinants of immunity to influenza infection in man. *Br. Med. Bull.* **35**, 69–75 (1979).
- Bachmann, M. F., Odermatt, B., Hengartner, H. & Zinkernagel, R. M. Induction of long-lived germinal centers associated with persisting antigen after viral infection. *J. Exp. Med.* **183**, 2259–2269 (1996).
- Sah, H. A new strategy to determine the actual protein content of poly(lactide-co-glycolide) microspheres. *J. Pharm. Sci.* **86**, 1315–1318 (1997).

Supplementary Information is linked to the online version of the paper at www.nature.com/nature.

Acknowledgements We thank R. Ahmed and B. Rouse for discussion and comments on the manuscript. We thank B. Norris for assistance with FACS analysis, and H. Oluoch for assistance with cryostat sectioning. The work in the laboratory of B.P. was supported by grants U54AI057157, R37AI48638, R01DK057665, U19AI057266, HHSN266200700006C, N01 AI50025 and U19AI090023 from the National Institutes of Health and a grant from the Bill & Melinda Gates Foundation. Work in A.G.-S. laboratories was partly funded by grants HHSN266200700010C, U54AI57158) and U01AI070469 from the National Institutes of Health.

Author Contributions S.P.K. and B.P. designed the study, planned the experiments and analysed the data. B.P. and S.P.K. wrote the manuscript. S.P.K., I.S. and B.P. designed and performed the H1N1 vaccine studies in mice and primates. D.K. assisted with the H1N1 vaccine studies in mice and primates. R.A.A., A.G.-S. and J.S. designed and performed the neutralization assays and challenge experiments with H5N1 vaccine studies in mice. T.H. and R.R. assisted with experiments. H.I.N. performed the microarray analysis. S.S. and M.A. designed and carried out the SPR-based avidity experiments. M.K. assisted with design and execution of mice and non-human primate experiments. N.M. assisted with design of formulations. J.J. assisted with immunohistochemistry and design of experiments. R.J.H. expressed and purified the recombinant H5HA protein. R.C. helped plan and design the H1N1 vaccine study in mice and primates.

Author Information All microarray data are deposited in the Gene Expression Omnibus under accession number GSE25677. Reprints and permissions information is available at www.nature.com/reprints. The authors declare no competing financial interests. Readers are welcome to comment on the online version of this article at www.nature.com/nature. Correspondence and requests for materials should be addressed to B.P. (bpulend@emory.edu).

METHODS

Encapsulation of antigens and TLR ligands in nanoparticles. Antigens were encapsulated in PLGA nanoparticles using a water in oil (w/o/w) emulsion technique. Briefly, 200 μ l of protein solution (PBS + 0.5% polyvinyl alcohol (PVA) as an excipient (Sigma Aldrich)), OVA grade VI (Sigma Aldrich) at 50 mg ml⁻¹, *Bacillus anthracis* PA (List Laboratories) at 15 mg ml⁻¹, and A/Vietnam/1203/2004 specific haemagglutinin protein (H5HA; affinity chromatography purified from 293 HEK cells) at 15 mg ml⁻¹ were homogenized with 10% w/v PLGA (RG502H, Bohringer Ingelheim) in dichloromethane (200 mg in 2 ml) with the Powergen homogenizer (Fisher Scientific) at speed 5 for 1.5 min. The water in oil emulsion (w/o) was then added to 15 ml of 5% w/v solution of PVA for the second emulsion step identical to the first emulsion process described earlier, at speed 5. The water in oil in water (w/o/w) double emulsion was then subjected to solvent evaporation for 4 h at room temperature (25 °C).

MPL was encapsulated in PLGA formulations using an oil in water (o/w) single emulsion process as described before with slight modifications⁸. MPL (detoxified lipid A, Avanti Lipids) was dissolved in chloroform at 5 mg ml⁻¹ and TLR7 ligand R837 (Invivogen) was dissolved at 10–20 mg ml⁻¹ in DMSO with heating. R848 was dissolved at 12.5 mg ml⁻¹ in dichloromethane. MPL, 0.5 ml at 5 mg ml⁻¹ was added to 200 mg of PLGA polymer dissolved in 2.0 ml of dichloromethane. For particles containing both MPL and R837, 0.5 ml or 5 mg of R837 in DMSO was added to the mixture of PLGA and MPL. For particles containing both MPL and R848, 8 mg of R848 in dichloromethane was added to the mixture of PLGA and MPL. For particles used in non-human primate studies, 0.1 ml of 5 mg ml⁻¹ MPL, 0.5 ml or 10 mg of R837 and 12.5 mg of R848 was added to 200 mg of PLGA polymer in 2.0 ml of dichloromethane. The organic phase containing PLGA with MPL and/or R837 or R848 was homogenized with 15 ml of a 5% w/v PVA solution for 2 min using a speed setting 6 at room temperature. The oil in water emulsion (o/w) was then added to 85 ml of a 5% w/v solution of PVA surfactant to evaporate the organic solvent for 4 h at room temperature. The nanoparticles formed were centrifuged at 3,500g for 20 min and washed with 50 ml of 0.2- μ m filter sterilized, deionized water 3 times. Nanoparticles were snap frozen in liquid nitrogen and lyophilized using a Freezone 2.5L benchtop lyophilizer (Labconco).

Nanoparticle characterization. Sizing of the nanoparticles was conducted using a dynamic light scattering based sizer (90PLUS) from Brookhaven Instruments. Sizes are represented as the mean diameter of the volume average size distribution \pm standard deviation of different batches. Protein encapsulation levels were estimated as described before using a BCA assay (Pierce Biotechnology)³¹. UV-Vis scan using a Cary Win50 UV-Vis spectrophotometer yielded a peak absorbance for R837 at 325 nm (327 nm for R848) and encapsulation was estimated using a standard curve of R837 or R848 in DMSO and NaOH/SDS. MPL encapsulated in nanoparticles was used in splenic dendritic-cell stimulation experiments with known concentrations of soluble MPL yielding identical cytokine production and estimated at 100% encapsulation efficiency.

Mouse dendritic cell culture. CD11c⁺ dendritic cells were isolated from spleens of naive C57BL/6 mice. Spleens were digested with collagenase type IV (Worthington Chemicals), and CD11c⁺ cells were enriched by positive selection using anti mouse CD11c magnetic beads according to manufacturer's instructions (Miltenyi Biotech). Dendritic cells (1 \times 10⁶ cells ml⁻¹) were cultured in 48-well culture plates with PLGA-encapsulated TLR ligands for 24 h.

Mice. *Il6*^{-/-} and *Ticam1*^{1ps2/1ps2} strains were obtained from Jackson Labs. *Ifnar*^{-/-} strain was obtained from S. Speck; *MyD88*^{-/-} and *Tlr7*^{-/-} from S. Akira; *Tlr4*^{-/-} from K. Kobayashi.

Immunization of mice and non-human primates. Eight-to-twelve week old BALB/c or C57BL/6 mice (Charles River Laboratories) were immunized with 10 μ g of antigen in nanoparticles (suspended in 200 μ l of PBS) subcutaneously at the base of the tail. TLR ligands were co-delivered with protein-encapsulated nanoparticles. Three milligrams of PLGA particles containing MPL, R837 or MPL+R837 containing 37.5 μ g of MPL and 60 μ g of R837 were used. Imject Alum (Pierce/ThermoScientific) was used to adsorb protein at a 1:1 volume ratio as per the manufacturer's instructions. Mice were bled via the lateral tail vein at regular intervals after primary and secondary immunizations and serum was isolated for analysis of antibody responses by ELISA assays. CD11c⁺ DTR mice¹³ were immunized 24 h after dendritic-cell depletion. Langerin-DTR mice¹⁴ were immunized 3 weeks after depletion, when there is replenishment of Langerin⁺ dendritic cells in the dermis and lymph nodes, but not in the epidermis³². CD4⁺ T cells were depleted with an anti-mouse CD4⁺ antibody (clone GK1.5, provided by R. Mittler) injected at 250 μ g per mouse as described³³. Ten-to-thirteen year old female Rhesus Macaques (7–10 kg) were used. Animals were immunized subcutaneously in the right leg. All animal procedures were performed in accordance with guidelines established by the Emory School of Medicine Institutional Animal Care and Use Committee Guidelines.

Antibody ELISA. Ninety-six-well Nunc maxisorp plates were coated with 100 μ l of 20 μ g ml⁻¹ of OVA, 1 μ g ml⁻¹ of PA or 0.5 μ g of H5HA protein overnight at 4 °C. Plates were washed 3 times with PBS/0.5% Tween-20 using a Biotek auto plate washer and blocked with 200 μ l of 4% non-fat dry milk (Biorad) for 2 h at room temperature. Serum samples from immunized mice at the indicated time points were serially diluted in 0.1% non-fat dry milk in PBS/0.5% Tween-20 and incubated on blocked plates for 2 h at room temperature. Detection antibodies were obtained from Southern Biotech. Wells were washed and incubated with anti-mouse IgG2c-HRP (horseradish peroxidase) conjugate (1:2,000), anti-mouse IgG2b-biotin conjugate (1:2,000), anti-mouse IgG1-HRP conjugate (1:5,000) and streptavidin-HRP conjugate (1:5,000) in PBS/0.5% Tween-20 for 2 h at room temperature. Plates were washed and developed using 100 μ l per well of tetramethylbenzidine (TMB) substrate (BD Biosciences) and stopped using 2N H₂SO₄. Plates were analysed using a BioRad plate reading spectrophotometer at 450 nm with correction at 595 nm. Antibody titres were represented as serum reciprocal dilution yielding a \geq 0.1 optical density (OD) value at 450 nm. Antibody levels (ng ml⁻¹) in H1N1 WIV-immunized mice were assayed as previously described³⁴. To analyse WIV-specific antibody levels in rhesus macaques, the assay was performed as described for mice. A capture rhesus IgG (clone SB108A) was used to establish a standard curve with the rhesus IgG standards (catalogue no. 0135-01; Southern Biotech). 2 μ g ml⁻¹ of WIV was used to coat Nunc maxisorp plates overnight and plates were blocked with 4% non-fat dry milk. Rhesus plasma samples were used at appropriate dilutions for prime and boost and incubated for 2 h at room temperature. Plates were washed 5 \times with PBS/0.5% Tween-20 using an automated plate washer and a goat anti-rhesus HRP was used at 1:4,000 dilution for 1 h at room temperature, washed and developed with TMB substrate. Antibody concentrations were calculated from the IgG standard curves and represented as μ g per ml.

BIAcore assay. SPR binding measurements were carried out on a BIAcore 3000 instrument (BIAcore/GE Healthcare), as described previously³⁵. Serum samples were injected at a 1:50 dilution in PBS for 5 min at a flow rate of 10 μ l min⁻¹. Binding to the negative control rPA surface was subtracted from each sample curve and binding response was measured at 15 and 500 s after the end of the injection. As a measure of antigen-specific antibody-binding avidity, maximal response unit (binding RU) and dissociation rates were measured. Maximal binding RU was measured after subtraction of non-specific signal on the control surface at 15 s post-injection and normalized dissociation was calculated as a ratio of late-to-early binding responses over a dissociation phase of 500 s. Following each injection cycle, chip surfaces were regenerated with a short injection of 25 mM NaOH.

H5N1 microneutralization assays. Serum samples from H5HA-immunized mice were tested for their ability to neutralize a recombinant (6:2) A/PR/8/34 influenza A virus expressing the A/Vietnam/1203/2004 H5HA and N1NA in cell culture *in vitro* as described previously²⁵.

Histology and immunofluorescence. Draining inguinal lymph nodes were isolated and snap frozen in moulds containing OCT medium, dropped into 2-methyl butane cooled with liquid nitrogen. Frozen lymph nodes were sectioned at 5 μ m, fixed in ice-cold acetone for 10 min, air dried and stored at -80 °C. Sections were fluorescently stained with Dylight488-labelled anti-mouse total IgG (Jackson ImmunoResearch), Alexa647-labelled anti-mouse B220 or GL-7 (Ebioscience), followed by Alexa555-conjugated streptavidin (Invitrogen). Fluorescent images were captured using the \times 5 and \times 20 objectives on a Zeiss Axioscope (Carl Zeiss).

B-cell ELISPOT. 1 \times 10⁶ lymph node cells were serially diluted and cultured overnight in duplicate wells of OVA-coated nitrocellulose-lined 96-well MAHA ELISPOT plates (Millipore). Cells were discarded and wells were treated with biotinylated goat anti-mouse total IgG (Southern Biotech) in assay buffer (PBS/0.5% Tween-20 + 1% FBS) for 1.5 h at room temperature. Wells were washed and treated with streptavidin alkaline phosphatase (Vector Labs) at 1:500 for 1.5 h at room temperature. NBT/BCIP colorimetric substrate for alkaline phosphatase was added to the wells and the reaction was stopped after visualization of purple coloured spots. Number of ELISPOTS per well were counted using an ImmunoSpot ELISPOT reader and represented as number of ELISPOTS (antibody-secreting cells) per total 1 \times 10⁶ lymph node cells.

CD4⁺ T-cell assays. 1 \times 10⁶ lymph node cells were cultured in a 200 μ l volume with 100 μ g ml⁻¹ of OVA protein or 5 μ g ml⁻¹ of PA or 5 μ g ml⁻¹ of H5HA in 96-well round-bottomed plates for 4 days. Cells were transferred to anti-CD3 (10 μ g ml⁻¹) and anti-CD28 (2 μ g ml⁻¹) coated flat-bottomed 96-well plates for 6 h in the presence of Golgi Plug (1 μ g ml⁻¹) (BD Biosciences). Cells were stained for surface CD4 using PerCP anti-mouse CD4 (clone RM4-5) for 30 min at 4 °C. Cells were washed 3 times with FACS buffer, fixed and permeabilized using BD Cytofix/Cytoperm and stained for intracellular IFN- γ using APC-conjugated anti-mouse IFN- γ (clone XMG1.2) for 30 min in 1 \times BD perm/wash solution at 4 °C. Cells were washed with perm wash followed by FACS buffer and acquired on a

FACS Caliber cytometer. FACS data were analysed using the Flow Jo software (Tree Star).

CD8⁺ T-cell assays. Primary and memory CD8⁺ T-cell responses were evaluated at day 7 after primary and secondary immunizations. Briefly, peripheral blood mononuclear cells (PBMCs) were enriched using a sucrose density gradient separation (Histopaque; Sigma Aldrich) and cultured with OVA-specific MHC class I restricted peptide at $1 \mu\text{g ml}^{-1}$ (SIINFEKL) for restimulation *ex vivo* in the presence of brefeldin A ($5 \mu\text{g ml}^{-1}$). Stimulated cells were stained for intracellular cytokines using established protocols from BD Biosciences as explained for CD4⁺ T-cell staining experiments above. Cells were stained with PerCP-conjugated anti-mouse CD8 α (Ly-2) (clone 53-6.7), APC-conjugated anti-mouse IFN- γ (clone XMG1.2), FITC-conjugated anti-mouse TNF- α (clone MP6-XT22) and PE-conjugated anti-mouse IL-2 (clone JES6-5H4). Labelled cells were acquired on a FACS Caliber cytometer and FACS data were analysed using Flow JO software (TreeStar).

B-cell multicolour flow cytometry. Antibodies used: PE-labelled anti-mouse IgG (Jackson Immunoresearch); PerCP-labelled anti-mouse CD19 (clone 6D5; Biolegend); E-fluor-405-labelled anti-mouse IgD (Ebioscience); Alexa430 succinimidyl ester for live/dead cell discrimination (Invitrogen); biotin-conjugated anti-mouse Ly77/GL7 (clone GL-7; Ebioscience); APC-labelled anti-mouse CD138 (clone 281-2; BD Biosciences); APC-Cy7-labelled anti-mouse TCR- β (clone H57-597; Biolegend); and APC-Cy7-labelled anti-mouse CD11b (clone M1/70, Biolegend). OVA was labelled with Alexa488 2,3,5,6 TFP ester (Invitrogen) as per the manufacturer's instructions. Unlabelled dye was separated using a 30K cut-off membrane-specified Amicon Ultra4 centrifugal filter (Millipore). Briefly, collagenase-digested lymph nodes from immunized mice were counted for absolute cell numbers. Cells were first stained with Alexa430 succinimidyl ester for dead-cell staining in PBS for 30 min at 4 °C. Cells were washed 2 times with FACS buffer (PBS with 5% FBS) and stained with PE-labelled anti-mouse total IgG for 30 min at 4 °C. Cells were washed 2 times and labelled with the all the above mentioned anti-mouse surface proteins. Qdot655-labelled streptavidin was used to label the biotinylated anti-mouse GL-7 antibodies for another 30 min at 4 °C. Stained cell samples were fixed with BD Cytfix (BD Biosciences) and acquired on a LSR-II cytometer (BD Biosciences). FACS data were analysed on Flow JO software. For B-cell sorting assays, cells were fluorescently labelled as described above and sorted on a FACS Aria cell sorter (BD Biosciences).

H1N1 virus stock preparation. Madin-Darby canine kidney (MDCK) cells (ATCC CCL 34, American Type Culture Collection) were maintained in DMEM (Mediatech) containing 10% FBS. Stocks of influenza virus strains were prepared by inoculation with H1N1 swine-origin A/California/04/09 strain in allantoic fluid, in 10- or 11-day-old embryonated hen's eggs. Virus stocks were harvested from the allantoic fluid. The purity of the virus was determined by SDS-PAGE in combination with Coomassie blue stain and electron microscopy. The HA activity was determined using chicken red blood cells 0.5% w/v in PBS pH 7.2 as previously described³⁶. The purified virus was inactivated with formaldehyde at a final concentration of 0.01% (v/v), incubated for 72 h at 4 °C, and then dialysed against PBS buffer. Inactivation of virus was confirmed by inoculation of the virus into 10-day-old embryonated hen's eggs and plaque assay in MDCK cells³⁷. We generated mouse adapted A/California/04/09 virus by five serial passages in BALB/c mice. We then determined the LD₅₀ for this virus using the Reed-Muench formula³⁸. For the challenge and infection studies the mice were anaesthetized with isoflurane and then infected with virus by intranasal instillation.

H1N1 HA inhibition assays. Determined as described previously³⁴.

H5N1 and H1N1 lethal challenge infections. Female BALB/c mice immunized with the indicated vaccine schedule were anaesthetized by intraperitoneal injection of ketamine/xylazine and then intranasally infected with 1,000 LD₅₀ of recombinant A/Vietnam/1203/2004 within the enhanced BSL3 Emerging Pathogens Facility at Mount Sinai School of Medicine. To determine survival rates post challenge with mouse adapted A/California/04/09 H1N1 virus, 5 female BALB/c mice per treatment group were challenged 8 weeks after immunization by intranasal instillation of 30 μl of $20 \times \text{LD}_{50}$ live virus after anaesthesia with isoflurane and monitored for morbidity and mortality up to 14 days. Animals were humanely killed and reported as dead if body weight loss achieved 25%. All H5N1 animal procedures were performed in accordance with guidelines established by the Mount Sinai School of Medicine Institutional Animal Care and Use Committee and National Institutes of Health for the care and use of laboratory animals.

H1N1 neutralization assays with primate plasma. Sera from non-human primates immunized with swine-origin H1N1 2009 were serially diluted and mixed with 100 p.f.u. of MDCK-grown homologous virus for 1 h at room temperature. The mixture was further added to an MDCK-cell monolayer and incubated for 45 min at room temperature. The inoculum was removed, wells were overlaid with DMEM agar and incubated for 2 days at 37 °C in a 5% CO₂ humidified incubator. Then plates were fixed with 0.25% glutaraldehyde and stained with 1% crystal violet

in 20% ethanol, and plaques were counted. Neutralizing antibody titres were determined as the reciprocal of the serum dilution that decreased by 50% the number of plaques formed by the live virus.

Affymetrix GeneChip analysis. Total RNA from sorted B cells (1.8×10^4 to 1.2×10^6 cells) was purified using Trizol (Invitrogen). All RNA samples were checked for purity using a ND-1000 spectrophotometer (NanoDrop Technologies) and for integrity by electrophoresis on a 2100 BioAnalyser (Agilent Technologies). The samples were amplified using the Nugen WT Pico Kit (NuGEN Technology) and the target reactions were run with 50 ng of total RNA. The amplification products were processed through the EXON Module (NuGEN Technology), which creates sense-strand cDNA targets. The sense-strand cDNA targets were then fragmented and labelled using NuGEN's FL-Ovation cDNA Biotin Module V2 (NuGEN Technology). Labelled targets were hybridized to GeneChip Mouse Gene 1.0ST arrays (Affymetrix), following standard Nugen protocols for target hybridization to the Affymetrix Gene Arrays. The hybridizations were run for 16 h at 45 °C, 60 r.p.m. in an Affymetrix Hybridization Oven 640. The Cartridge arrays were washed and stained using the Affymetrix Fluidics Stations 450, following Affymetrix protocols. Scanning was performed on an Affymetrix GeneChip 3000 7G scanner, and Affymetrix GCOS software was used to perform image analysis and generate raw intensity data. Two independent sets of samples at day 7 post-treatment were used in our analyses. Each set is comprised of B cells from mice immunized with MPL+R837 or from those immunized with antigen plus MPL or R837 alone. Probe sets of all six samples were normalized by RMA, which includes global background adjustment and quantile normalization. Each set of samples was subsequently normalized by z-score (number of standard deviations from mean) and treated as biological replicates. Affymetrix chip annotation of GeneChip Mouse Gene 1.0ST platform was used to annotate and select probe sets that target a known gene (defined as having an Entrez gene ID). Different probe sets that target the same gene were collapsed by taking the probe set with the highest median expression value across all samples. Student's *t*-test ($P < 0.05$) was used to identify genes differentially expressed in mice immunized with antigen plus MPL+R837 compared to those immunized with antigen plus MPL or R837 alone. A meta-analysis was performed using publicly available microarray data of distinct B-cell subsets (plasma, germinal centre and memory B cells)²³. Purification strategy, RNA-processing method and hybridization strategy can be found in the original publication²³. Raw microarray data (CEL files of samples GSM94747, GSM94762, GSM94763, GSM94764, GSM94765, GSM94766, GSM94767, GSM94768, GSM94769, GSM94771 and GSM94772) were downloaded from the NCBI GEO website (GSE4142) and processed by RMA normalization. Affymetrix chip annotation of the GeneChip Mouse Genome 430 2.0 platform was used to annotate and select probe sets that target a known gene (defined as having an Entrez gene ID). Different probe sets that target the same gene were collapsed by taking the probe set with the highest median expression value across all samples. Student's *t*-test ($P < 0.05$) was used to identify differentially expressed genes (DEGs) between any given two B-cell subsets. Genes were classified as 'plasma DEGs' if they were upregulated in plasma compared to germinal-centre B cells and also upregulated in plasma compared to memory B cells. A similar approach was used to identify 'germinal center DEGs' and 'memory DEGs'.

Genes that were up- or downregulated in mice immunized with antigen plus MPL+R837 compared to those immunized with antigen plus MPL or R837 alone, were cross-referenced to the genes highly expressed in specific B-cell subsets. Fold enrichment was calculated using the formula (common ZX/deg Z)/(subset X/total), where common ZX = number of genes upregulated in treatment Z (combination of MPL+R837 or individual MPL or R837) and also highly expressed in B-cell subset X; deg Z = number of all genes upregulated in treatment Z; subset X = number of all genes highly expressed in B-cell subset X; and total = number of all genes in the chip common to both platforms. In Supplementary Figure 11a, the labelled genes on the right indicate highly expressed genes in the MPL+R837 group that are known to regulate B-cell survival, the germinal-centre response, and differentiation of memory B cells³⁹⁻⁵⁶.

32. Henri, S. *et al.* CD207⁺ CD103⁺ dermal dendritic cells cross-present keratinocyte-derived antigens irrespective of the presence of Langerhans cells. *J. Exp. Med.* **207**, 189–206 (2010).
33. den Haan, J. M., Kraal, G. & Bevan, M. J. Cutting edge: lipopolysaccharide induces IL-10-producing regulatory CD4⁺ T cells that suppress the CD8⁺ T cell response. *J. Immunol.* **178**, 5429–5433 (2007).
34. Zhu, Q. *et al.* Immunization by vaccine-coated microneedle arrays protects against lethal influenza virus challenge. *Proc. Natl Acad. Sci. USA* **106**, 7968–7973 (2009).
35. Staats, H. F. *et al.* *In vitro* and *in vivo* characterization of anthrax anti-protective antigen and anti-lethal factor monoclonal antibodies after passive transfer in a mouse lethal toxin challenge model to define correlates of immunity. *Infect. Immun.* **75**, 5443–5452 (2007).
36. Compans, R. W. Hemagglutination-inhibition: rapid assay for neuraminic acid-containing viruses. *J. Virol.* **14**, 1307–1309 (1974).

37. Enioutina, E. Y., Visic, D. & Daynes, R. A. The induction of systemic and mucosal immune responses to antigen-adjuvant compositions administered into the skin: alterations in the migratory properties of dendritic cells appears to be important for stimulating mucosal immunity. *Vaccine* **18**, 2753–2767 (2000).
38. Reed, L. J. & Muench, H. A simple method of estimating fifty percent endpoints. *Am. J. Hyg.* **27**, 493–497 (1938).
39. Badr, G. *et al.* Type I interferon (IFN- α/β) rescues B-lymphocytes from apoptosis via PI3K δ /Akt, Rho-A, NF κ B and Bcl-2/Bcl(XL). *Cell. Immunol.* **263**, 31–40 (2010).
40. Bekeredjian-Ding, I. B. *et al.* Plasmacytoid dendritic cells control TLR7 sensitivity of naive B cells via type I IFN. *J. Immunol.* **174**, 4043–4050 (2005).
41. Thibault, D. L. *et al.* IRF9 and STAT1 are required for IgG autoantibody production and B cell expression of TLR7 in mice. *J. Clin. Invest.* **118**, 1417–1426 (2008).
42. Tovey, M. G., Lallemand, C. & Thyphronitis, G. Adjuvant activity of type I interferons. *Biol. Chem.* **389**, 541–545 (2008).
43. Swanson, C. L. *et al.* Type I IFN enhances follicular B cell contribution to the T cell-independent antibody response. *J. Exp. Med.* **207**, 1485–1500 (2010).
44. Liu, H. *et al.* Functional studies of BCL11A: characterization of the conserved BCL11A-XL splice variant and its interaction with BCL6 in nuclear paraspeckles of germinal center B cells. *Mol. Cancer* **5**, 18 (2006).
45. Smith, K. G. *et al.* *bcl-2* transgene expression inhibits apoptosis in the germinal center and reveals differences in the selection of memory B cells and bone marrow antibody-forming cells. *J. Exp. Med.* **191**, 475–484 (2000).
46. Aiba, Y. *et al.* Preferential localization of IgG memory B cells adjacent to contracted germinal centers. *Proc. Natl Acad. Sci. USA* **107**, 12192–12197 (2010).
47. Zhou, G. & Ono, S. J. Induction of *BCL-6* gene expression by interferon- γ and identification of an IRE in exon I. *Exp. Mol. Pathol.* **78**, 25–35 (2005).
48. Mitsdoerffer, M. *et al.* Proinflammatory T helper type 17 cells are effective B-cell helpers. *Proc. Natl Acad. Sci. USA* **107**, 14292–14297 (2010).
49. Chin, A. I. *et al.* TANK potentiates tumor necrosis factor receptor-associated factor-mediated c-Jun N-terminal kinase/stress-activated protein kinase activation through the germinal center kinase pathway. *Mol. Cell. Biol.* **19**, 6665–6672 (1999).
50. Basso, K. & Dalla-Favera, R. BCL6: master regulator of the germinal center reaction and key oncogene in B cell lymphomagenesis. *Adv. Immunol.* **105**, 193–210 (2010).
51. Kano, G. *et al.* Ikaros dominant negative isoform (Ik6) induces IL-3-independent survival of murine pro-B lymphocytes by activating JAK-STAT and up-regulating Bcl-xl levels. *Leuk. Lymphoma* **49**, 965–973 (2008).
52. Ke, N., Godzik, A. & Reed, J. C. Bcl-B, a novel Bcl-2 family member that differentially binds and regulates Bax and Bak. *J. Biol. Chem.* **276**, 12481–12484 (2001).
53. Airoidi, I. *et al.* Expression and function of IL-12 and IL-18 receptors on human tonsillar B cells. *J. Immunol.* **165**, 6880–6888 (2000).
54. Airoidi, I. *et al.* Heterogeneous expression of interleukin-18 and its receptor in B-cell lymphoproliferative disorders deriving from naive, germinal center, and memory B lymphocytes. *Clin. Cancer Res.* **10**, 144–154 (2004).
55. Hikida, M. *et al.* PLC- γ 2 is essential for formation and maintenance of memory B cells. *J. Exp. Med.* **206**, 681–689 (2009).
56. Nera, K. P. & Lassila, O. Pax5—a critical inhibitor of plasma cell fate. *Scand. J. Immunol.* **64**, 190–199 (2006).

Klotho suppresses RIG-I-mediated senescence-associated inflammation

Feng Liu^{1,2}, Su Wu^{1,2}, Hongwei Ren¹ and Jun Gu^{1,3,4}

It is well known that aged or senescent cells develop a complex senescence-associated secretory phenotype (SASP), which is observed both in culture and *in vivo*. However, the mechanisms underlying the induction of the SASP are largely unknown. We demonstrate that retinoic-acid-inducible gene-I (RIG-I) is induced through the ataxia telangiectasia mutated–interferon regulatory factor 1 (ATM–IRF1) axis in senescent cells and that RIG-I signalling mediates the expression of two important mediators of inflammation, interleukin-6 (IL-6) and IL-8. Klotho has been associated with ageing. We show here that the intracellular, but not the secreted, form of klotho interacts with RIG-I and that this interaction inhibits RIG-I-induced expression of IL-6 and IL-8 both *in vitro* and *in vivo*. Our study uncovers a mechanism in which klotho functions as an anti-ageing factor through the suppression of RIG-I-mediated inflammation.

When maintained in culture conditions that enable their continuous replication, normal human fibroblasts eventually lose their proliferative capacity after a finite number of cell divisions¹. Such cellular senescence occurs in response to excessive extracellular and intracellular stress and is characterized by the inability of cells to proliferate despite the presence of abundant nutrients and mitogens, and by the preservation of cell viability and metabolic activity. Senescence can be triggered by many different stimuli, including DNA damage, expression of oncogenes, oxidative stress and mitogenic signals^{2,3}, and during this process a large number of soluble factors involved in intracellular signalling are secreted^{4,5}. One key observation made in ageing human fibroblasts is the upregulation of cytokines and chemokines and their receptors⁶. Further evidence for increased production of inflammatory mediators during ageing comes from two recent reports that demonstrate that IL-6 and IL-8 and their receptors play a key role in the establishment and maintenance of the senescence phenotype^{4,7}. Furthermore, in human colon adenomas, increased IL-8 expression was detected in areas showing features of senescence (p16^{INK4a} positive and Ki-67 negative), indicating that induction of inflammation contributes to senescence *in vivo*^{4,7,8}.

Klotho (*kl*) is a recently identified gene related to ageing⁹. Deficiency of *kl* in mice causes a syndrome resembling human ageing including arteriosclerosis, osteoporosis, endothelial dysfunction, Parkinsonian gait and cognitive impairment^{9–12}. Alternative splicing at the RNA level results in two transcripts of the *kl* gene. One encodes a single-pass membrane form of the protein, whereas the other transcript encodes a

putative secreted form that acts as a humoral factor^{13–15}. In humans, the secreted form of klotho (KLMs) has a higher expression level than the membrane form (KLM; refs 14,16). The membrane form of klotho functions as an obligatory co-receptor for fibroblast growth factor 23 (FGF23), a bone-derived hormone that regulates the phosphate, calcium and vitamin D balance, and defects in either *kl* or *Fgf 23* cause phosphate retention and a premature-ageing syndrome in mice^{17,18}. The secreted form of klotho regulates activities of multiple ion channels and growth factors including insulin, insulin-like growth factor IGF-I and Wnt, and protects cells and tissues from oxidative stress through a mechanism yet to be identified^{19–24}. Thus, the transmembrane and secreted forms of klotho have distinct functions, which may collectively affect the ageing process in mammals.

RIG-I is a caspase recruitment domain (CARD)-containing protein that functions as a cytoplasmic RNA sensor²⁵. It induces type-I interferon through a Toll-like receptor 3 (TLR3)-independent pathway following interaction with double-stranded RNA viruses²⁶. The downstream signalling molecule, MAVS (mitochondrial antiviral signalling; also known as interferon- β promoter stimulator 1, IPS-1; virus-induced-signalling adapter, VISA; and Cardif), is located in mitochondria and functions as a RIG-I adaptor^{27–30}. In addition to its antiviral response, recent studies also demonstrate that RIG-I is involved in inflammation. Various chronic inflammatory diseases show evidence of increased levels of RIG-I, associated with increased levels of pro-inflammatory cytokines. The induction of these mediators occurs independently of TLR4 (ref. 31), MAVS or the Nod-like receptor

¹National Key Laboratory of Protein Engineering and Plant Gene Engineering, LSC, Peking University, Beijing 100871, China. ²These authors contributed equally to this work. ³Present address: Department of Biochemistry and Molecular Biology, College of Life Sciences, Peking University, Beijing 100871, China. ⁴Correspondence should be addressed to J.G. (e-mail: gj@pku.edu.cn)

Received 27 July 2010; accepted 11 January 2011; published online 20 February 2011; corrected online 16 March 2011; DOI: 10.1038/ncb2167

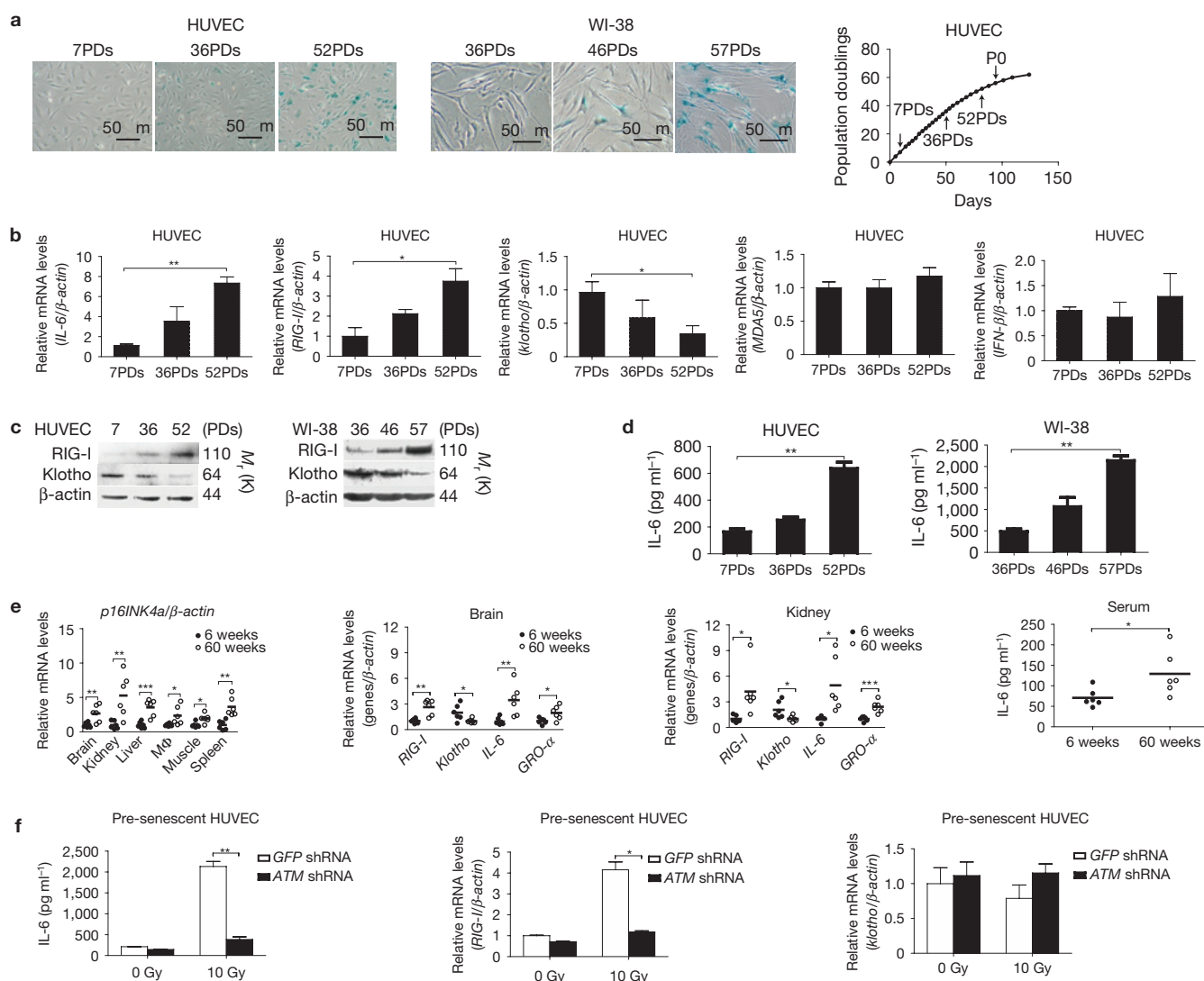


Figure 1 Correlation of induction of RIG-I with interleukins, and reduction of klotho in replicative senescent cells. **(a)** Senescence-associated β -galactosidase staining in HUVECs (left) and WI-38 (middle) cells with different population doublings (PDs). The growth curve (right) indicates the passage number (OPDs, 7PDs, 36PDs, 52PDs) of HUVECs used in this study. **(b,c)** Induction and reduction of genes at mRNA **(b)** or protein **(c)** level in HUVECs and WI-38 cells at indicated population doublings. **(d)** Supernatants from different passages of HUVECs and WI-38 cells were collected for IL-6 measurements by ELISA. Three independent cell populations in each passage were analysed in **b** and **d**. Error bars

represent means + s.d. ** $P < 0.01$. **(e)** Relative mRNA levels of $p16^{INK4a}$, *RIG-I*, *klotho*, *IL-6* and *GRO- α* in different tissues (M Φ , peritoneal macrophage) and serum IL-6 protein level, from young (6 weeks) and aged mice (60 weeks), were determined by qualitative PCR with reverse transcription and by ELISA. Six mice in each group were analysed ($n = 6$). The mRNA levels of *klotho* in the old group are considered as control. For other genes, mRNA levels in the young group are considered as control. **(f)** Relative mRNA levels and secreted IL-6 level in control and ATM-depleted pre-senescent HUVECs after irradiation. Error bars represent mean + s.d. ($n = 3$) * $P < 0.05$, ** $P < 0.01$, *** $P < 0.001$.

NLRP3 (ref. 32). Here, we report that senescence-induced expression of pro-inflammatory cytokines is mediated by RIG-I and this can be suppressed by the anti-ageing factor, klotho.

RESULTS

Induction of RIG-I and interleukins in senescence

It is well known that senescence is associated with increased levels of the interleukins IL-6 and IL-8 (refs 4,7), and the activation of the RIG-I signalling pathway results in increased IL-6 expression³³. To test whether RIG-I plays a role in inflammation associated with ageing, we measured the expression levels of RIG-I and IL-6 at various times during cellular senescence. Using both primary human umbilical vein endothelial cells

(HUVECs) and fibroblasts (WI-38), while cells underwent senescence (Fig. 1a), we observed that RIG-I was induced at both the messenger RNA (Fig. 1b) and protein (Fig. 1c) levels, correlating with the increase of IL-6 and IL-8 gene expression (Fig. 1b and Supplementary Fig. S1a) and secretion (Fig. 1d). The expression of melanoma differentiation-associated protein-5 (MDA5) did not change, and no changes were observed in the expression levels of interferon- β (IFN- β ; Fig. 1b). We next measured the expression levels of RIG-I and interleukins *in vivo* and found increased levels of RIG-I, IL-6 and growth-regulated oncogene- α (GRO- α) in various tissues including brain and kidney of 60-week-old mice ($n = 6$; Fig. 1e). The tissues of these aged mice all showed high-level expression of $p16^{INK4a}$, an ageing marker, whereas tissue from

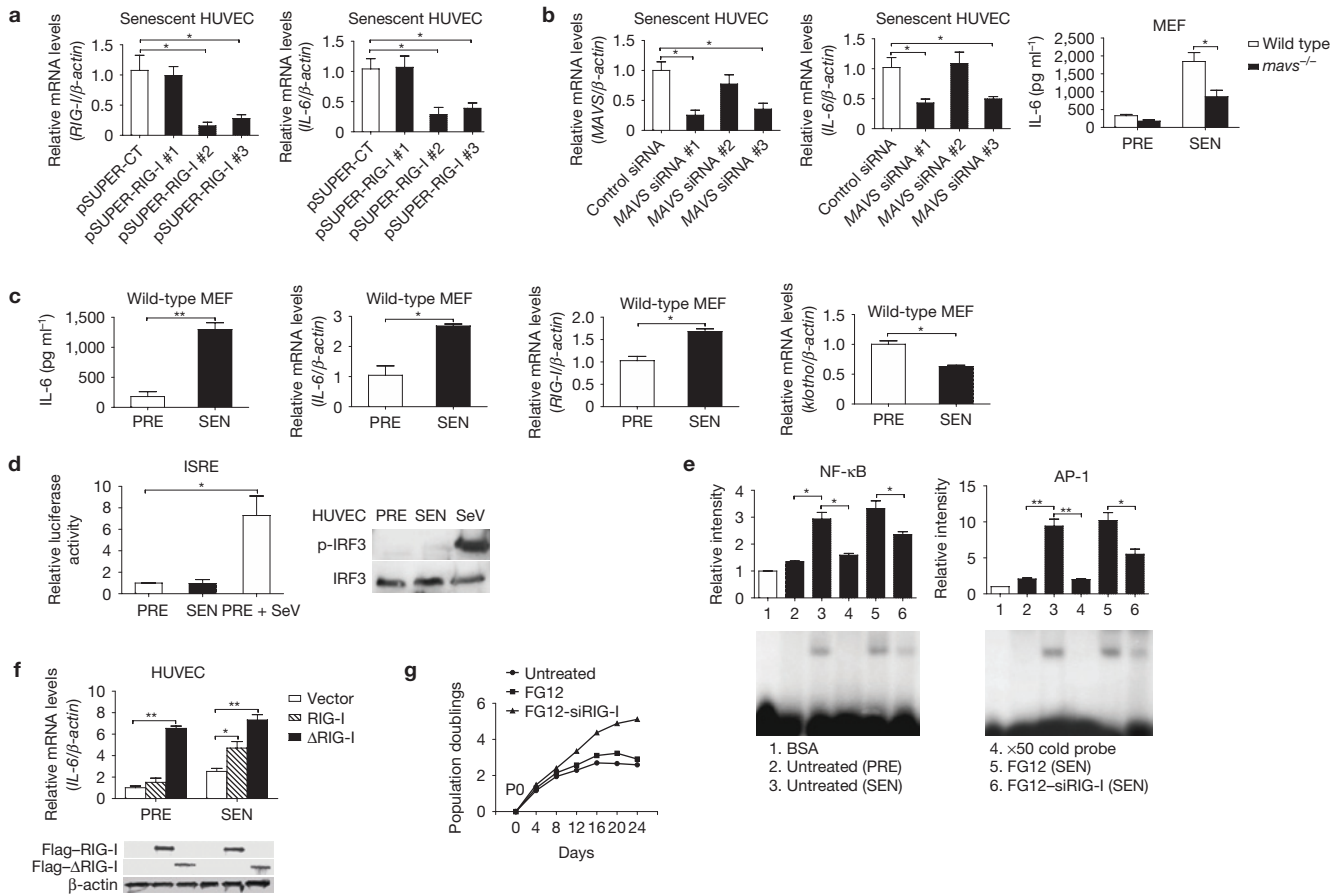


Figure 2 RIG-I signalling mediates senescence-associated inflammation. **(a)** Silencing of RIG-I by interference plasmids in senescent HUVECs blocks the expression and secretion of IL-6. Total RNA was extracted and subjected to qPCR. **(b)** Silencing of MAVS by siRNA in senescent HUVECs blocks the expression of IL-6 (left). Supernatants from the MEFs of wild-type mice and MAVS-knockout mice (*mavs*^{-/-}) at different passages and subjected to ELISA. MEFs of the primary passage (P0) and passage 4 (P4, 14 days after P0) were considered as pre-senescent (PRE) and replicative senescent (SEN) cells, respectively (right). **(c)** Gene expression of pre-senescent and senescent MEFs from wild-type mice. The supernatant of each MEF population was collected and subjected to ELISA for IL-6. Total RNA was extracted and subjected to qPCR for the indicated genes. Three independent cell populations in each passage were analysed above. Error bars represent means + s.d. * $P < 0.05$, ** $P < 0.01$. **(d)** IRF3 activity remains unchanged in senescent cells. Pre-senescent and senescent HUVECs were transfected with ISRE luciferase reporter plasmid, and 12 h after transfection cells were infected with Sendai virus as a positive control or left uninfected for another 12 h

before the luciferase assay was carried out (left). IRF3 phosphorylation was determined by western blot (right). **(e)** Enhanced NF- κ B and AP-1 activity in senescent cells. Nuclear proteins of pre-senescent and senescent HUVECs with treatments as indicated were extracted and subjected to EMSA (bottom) and quantified (top). Three independent experiments were analysed. Error bars represent means + s.d. * $P < 0.05$, ** $P < 0.01$. **(f)** RIG-I is activated in senescent cells. Pre-senescent and senescent HUVECs were transfected with similar amounts of Flag-RIG-I and Flag- Δ RIG-I (bottom). Total RNA and protein were extracted 24 h after transfection and IL-6 mRNA level determined by qPCR (top). In **d** and **f** error bars represent means + s.d. ($n = 3$). * $P < 0.05$, ** $P < 0.01$. **(g)** Growth curves of control HUVECs and RIG-I-depleted HUVECs. Senescent HUVECs were infected with lentivirus encoding an FG12 control plasmid or a RIG-I interference plasmid. HUVECs were passaged and the population doublings were determined by counting the cell number during each passage starting from the P0 point as shown in Fig. 1a. Representative growth curves of three independent experiments are shown. Untreated pre-senescent HUVECs are included as a control (lane 2).

young mice did not. It has been reported that persistent DNA damage response also triggers senescence-associated inflammation³⁴. Therefore, we tested whether irradiation-induced DNA damage induces RIG-I and IL-6, and found that cells treated with high-dose radiation (10 Gy) increased RIG-I expression and IL-6 secretion (Fig. 1f). Genotoxic stress by radiation or an oncogene induces the expression of interferon regulatory factor 1 (IRF1), dependent on the ataxia telangiectasia mutated (ATM) signalling pathway³⁵. To investigate whether increased expression of RIG-I and IL-6 during DNA damage depend on this pathway, we transfected cells with an ATM interference plasmid or a control vector and treated the cells with a high dose of irradiation. Knockdown of ATM prevented RIG-I and IL-6 induction (Fig. 1f),

indicating that, during persistent DNA damage, RIG-I and IL-6 expression occurs through activation of the ATM signalling pathway.

RIG-I signalling is required for senescence-associated inflammation

The co-induction of RIG-I and IL-6 in senescent cells *in vitro* and *in vivo* indicates that RIG-I may play a role in mediating the increased endogenous levels of IL-6 during ageing^{26,31,32}. To test this hypothesis, we transfected senescent HUVECs with several RNA interference vectors and show that RNAi vectors that effectively knocked down endogenous RIG-I also suppressed the expression and secretion of IL-6 and IL-8 (Fig. 2a and Supplementary Fig. S1b). To address whether

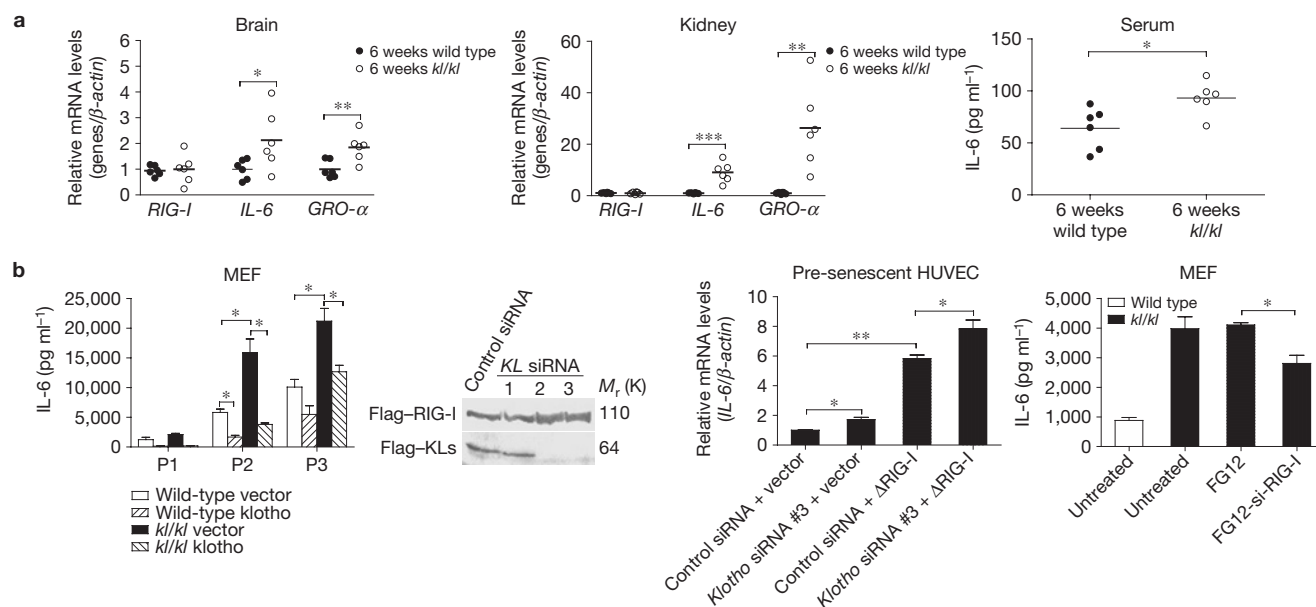


Figure 3 Endogenous klotho is a physiological inhibitor of RIG-I-mediated expression of IL-6. **(a)** Relative mRNA levels of *RIG-I*, *IL-6* and *GRO-α* in brain and kidney from wild-type and klotho-deficient (*kl/kl*) mice. Qualitative PCR results were obtained from RNA samples of six individual mice (left). Means of *RIG-I*, *IL-6* and *GRO-α* mRNA levels in the wild-type group were considered as control. Serum IL-6 levels in wild-type and *kl/kl* mice are shown (right). The ELISA result was obtained from independent serum samples of six mice for each group. \pm * $P < 0.05$, ** $P < 0.01$, *** $P < 0.001$. Black lines represent means **(b)** Supernatants from wild-type and klotho-deficient MEFs (*kl/kl*) were collected and subjected to ELISA for IL-6.

For the rescue experiment, MEFs were transfected with the mouse membrane form of klotho at different passage numbers. Supernatants were collected 24 h after transfection and subjected to ELISA (left). Pre-senescent HUVECs were transfected with empty vector, Δ RIG-I, control siRNA and klotho siRNA as indicated. Western blot (middle left) and qPCR (middle right) were carried out as described in the Methods. Wild-type and klotho-deficient MEFs were pretreated with control and RIG-I interference lentivirus separately. Supernatants were collected and subjected to ELISA for IL-6 (right). Three independent cell populations in each condition were analysed. Error bars represent means + s.d. * $P < 0.05$, ** $P < 0.01$.

RIG-I signalling is required for senescence-associated inflammation, we knocked down MAVS. Figure 2b shows that silencing of MAVS suppressed the expression of IL-6 in senescent cells, similarly to silencing of RIG-I. Wild-type mouse embryonic fibroblasts (MEFs) showed an increase in RIG-I following cell passage, and both mRNA and protein levels of IL-6 were found to be increased as well (Fig. 2c). In contrast, *MAVS*^{-/-} MEFs showed much lower levels of IL-6 following cell passage, despite increased levels of RIG-I. These data indicate that RIG-I signalling controls the expression of IL-6 during cell proliferation.

So far we have shown that activation of the RIG-I signalling pathway in senescent cells results in increased levels of IL-6 and IL-8, but not IFN- β (Fig. 1b). As RIG-I-mediated expression of IFN- β depends on the activation of interferon-stimulated response element (ISRE), we next addressed whether ISRE is activated in senescent cells. An ISRE reporter was transfected into pre-senescent or senescent cells. As shown in Fig. 2d, the ISRE was not activated by senescence, and the transcription factor IRF3 that recognizes ISRE was not activated either. These results indicate that the signalling pathways that mediated the expression of IFN- β are not activated during senescence, despite increased RIG-I expression. It is well known that the expression of inflammatory factors such as IL-6 and 8 mainly relies on the activation of nuclear factor- κ B (NF- κ B) and activator protein 1 (AP-1). We show that both NF- κ B and AP-1 were highly activated in senescent, but not in pre-senescent, cells (Fig. 2e). In addition, silencing RIG-I in senescent cells significantly reduced the activation of these two transcription factors (Fig. 2e), further supporting a key role for NF- κ B in RIG-I-induced expression of IL-6 and 8.

Several studies have identified that increased RIG-I expression is associated with inflammation^{31,36–39}. It has been demonstrated that CARD (Δ RIG-I, RIG-I aa1–230), the active form of RIG-I, can activate its signalling²⁵. To address whether the active form or RIG-I mediates the induction of IL-6 in senescent cells, we transfected RIG-I and Δ RIG-I into pre-senescent and senescent HUVECs and quantified the IL-6 levels by quantitative PCR (qPCR). Forced expression of RIG-I barely induced IL-6 in pre-senescent cells, whereas Δ RIG-I strongly induced the expression of IL-6. In contrast, RIG-I and Δ RIG-I induced comparable levels of IL-6 in senescent cells (Fig. 2f). These results indicate that in senescent cells induction of RIG-I alone led to the expression of inflammatory factors such as IL-6 and 8. Interestingly, knockdown of RIG-I in senescent HUVECs led to extension of the lifespan of the senescent cells (Fig. 2g), which indicates that RIG-I-induced inflammation plays a role in promoting and maintaining senescence. This is consistent with observations that inhibition of IL-6 and IL-8 extends the proliferative capacity of cultured cells passages^{4,5,7}.

Klotho suppresses RIG-I-mediated expression of IL-6 and IL-8

Klotho is known to be an anti-ageing protein²⁰, and has recently been reported to have an anti-inflammatory function⁴⁰. In this study we confirm that expression of klotho was decreased in senescent cells (Figs 1b,c and 2c) and in various tissues of aged mice (Fig. 1e). We further show that klotho-deficient mice show significantly higher IL-6 expression levels than wild-type mice ($n = 6$; Fig. 3a), indicating that klotho regulates age-related inflammation. To investigate this further, we measured the endogenous levels of IL-6 in klotho-deficient

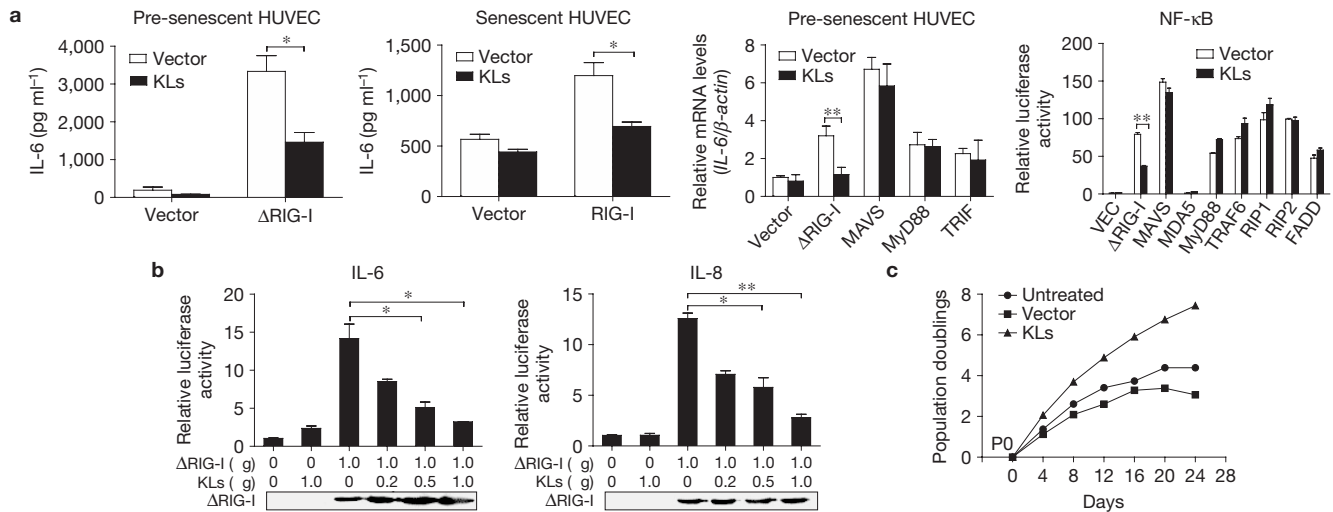


Figure 4 Klotho inhibits RIG-I-mediated activation of NF- κ B. (a) Pre-senescent HUVECs, senescent HUVECs and 293T cells (for luciferase assay) were transfected with plasmids as indicated. At 24 h after transfection, supernatant and total RNA were collected and subjected to analysis by ELISA (left and middle left), qPCR (middle right) and a reporter assay for NF- κ B activity, respectively. (b) 293T cells (for the luciferase assay) were transfected with IL-6 or IL-8 reporter plasmid, Δ RIG-I plasmid and the indicated amount of klotho plasmid, followed by luciferase assays

24 h after transfection (top of each panel). Δ RIG-I expression levels are shown in the bottom of each panel. In **a** and **b** error bars represent means + s.d. ($n = 3$). * $P < 0.05$, ** $P < 0.01$. (c) Growth curves of control HUVECs and klotho-overexpressing HUVECs. Senescent HUVECs were transfected with control plasmid or klotho-expression plasmid. HUVECs were passaged and the population doublings were determined by counting the cell number during each passage starting from the PO point as shown in Fig. 1a. Representative growth curves of three independent experiments are shown.

MEFs (*kl/kl*) *in vitro* and found higher IL-6 levels following cell passage, compared with wild-type MEFs (Fig. 3b). Overexpression of klotho in *kl/kl* MEFs resulted in similar IL-6 levels to wild-type MEFs, whereas klotho-deficient pre-senescent HUVECs showed silence of klotho in pre-senescent HUVECs showed higher IL-6 levels (Fig. 3b). Interestingly, knocking down endogenous RIG-I in *kl/kl* MEFs reduced IL-6 levels (Fig. 3b).

To investigate whether klotho regulates RIG-I-mediated inflammation, we transfected klotho and the active form of RIG-I (Δ RIG-I) into HUVECs. Overexpression of Δ RIG-I in pre-senescent HUVECs led to IL-6 secretion, whereas overexpression of klotho reduced the level of IL-6 (Fig. 4a). Expression of ectopic klotho in senescent HUVECs also blocked RIG-I-induced expression of IL-6 (Fig. 4a). As expression of cytokines can be mediated by different adaptor proteins, including Toll/Interleukin-1 receptor (TIR)-domain-containing adapter-inducing interferon- β (TRIF) and myeloid differentiation primary response protein (MyD88), we next co-transfected these adaptors with klotho in pre-senescent HUVECs, and measured the expression of IL-6 by qPCR. As shown in Fig. 4a, klotho inhibited only Δ RIG-I, and not MAVS-, TRIF- or MyD88-mediated expression of IL-6. Using a reporter assay to study the specific block role of klotho, we found that klotho specifically suppressed the activation of NF- κ B by Δ RIG-I, and not other signalling molecules including MAVS, MDA5, MyD88, tumour necrosis factor receptor-associated factor 6 (TRAF6), receptor interacting protein 1 (RIP-1), RIP-2 and Fas-associated death domain (FADD) protein (Fig. 4a). Further analysis showed that Δ RIG-I-mediated activation of the IL-6 and IL-8 promoters was suppressed by klotho in a dose-dependent manner. Finally, we tested whether klotho has a role in replicative senescence. Ectopic klotho was transfected into HUVECs followed by monitoring the replicative senescence. As shown

in Fig. 4c, ectopic expression of klotho in HUVECs extended their replicative potential.

RIG-I-mediated IL-6 and IL-8 are suppressed by intracellular klotho

Klotho has two forms, a secreted and a membrane form^{13,14}. KLS and KLM, respectively. To determine which form of klotho functions as the RIG-I suppressor, we first deleted the amino-terminal signal sequence of the secreted form of klotho (KLS Δ ss). As shown in Fig. 5a, deletion of the signal sequence resulted in a failure to secrete the protein. To test the effect of KLS and KLS Δ ss on RIG-I-mediated expression of interleukins, KLS and KLS Δ ss were co-transfected with Δ RIG-I, respectively, into 293T cells, which express both klotho and RIG-I as well as IL-6, and were subjected to the reporter assays. KLS and KLS Δ ss equally suppressed Δ RIG-I mediated activation of the IL-6, IL-8 and NF- κ B promoters (Fig. 5b), indicating that the effect on RIG-I-induced inflammation is mediated by the intracellular klotho. To further test whether the extracellular klotho affects RIG-I signalling, we used conditioned medium containing klotho. The full length of klotho (KLM) was transfected into 293T cells and its expression and secretion were confirmed by immunoblot analysis (Fig. 5c). As expected, the expression of KLM leads to the secretion of both the membrane form and soluble form⁴¹. KLS failed to affect RIG-I-induced activation of the IL-6 promoter, whereas the Wnt signalling was blocked (Fig. 5c), which confirmed the biological activity of KLS in our assay²¹. To further strengthen the results, KLM was co-transfected with Δ RIG-I in the presence of an antibody against klotho. The added antibody did not alleviate the inhibition of IL-6 production by overexpressed klotho (Fig. 5d). These data indicate that KLS does not function as a RIG-I suppressor, and that only the intracellular form of klotho is able to inhibit RIG-I-induced expression of IL-6.

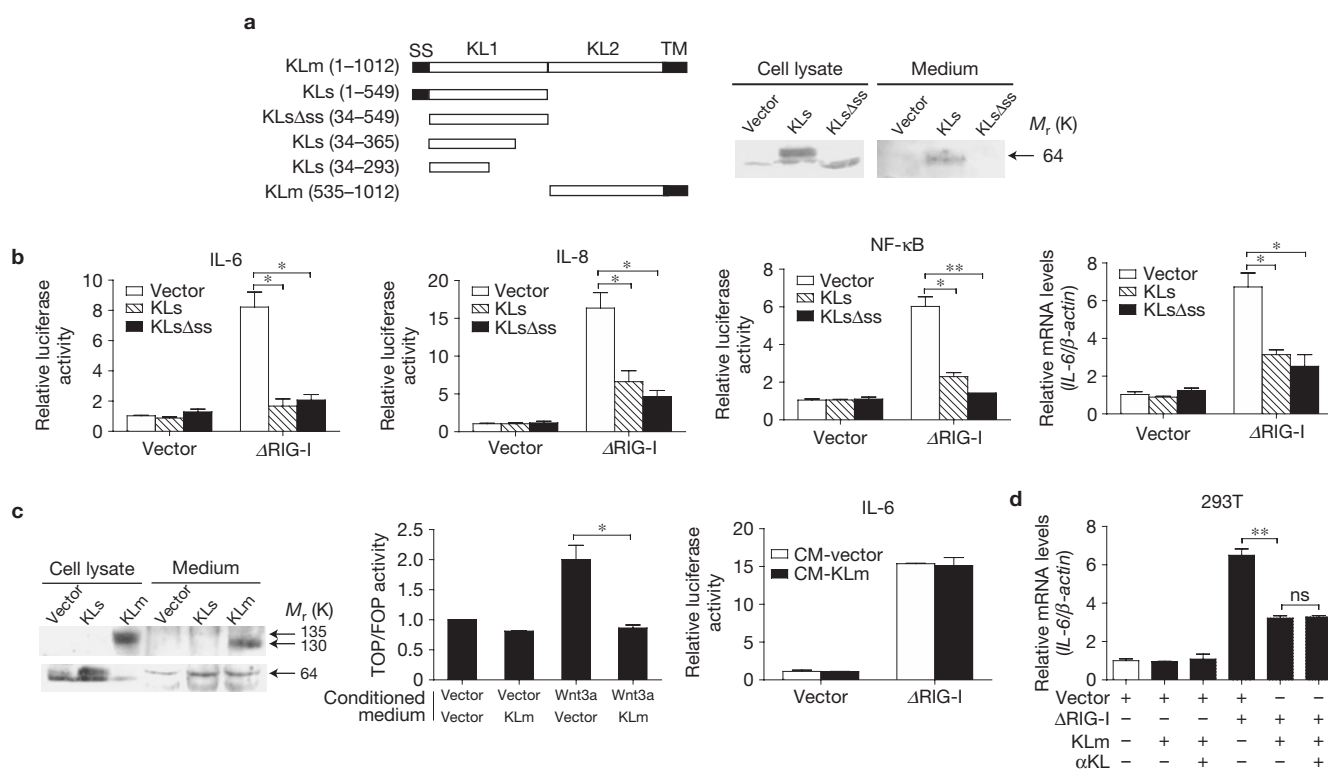


Figure 5 RIG-I-mediated expression of IL-6 and 8 is suppressed by intracellular, not secreted, klotho. **(a)** 293T cells were transfected with indicated KLotho and KLothoΔss constructs. Supernatant was collected 72 h after transfection by trichloroacetic acid methods. Total cell lysate and supernatant were analysed by immunoblotting with antibody against klotho (right). Different truncated klotho constructs are shown on the left. **(b)** KLothoΔss inhibits RIG-I-mediated IL-6 and IL-8 production. 293T cells were transfected with the indicated plasmids. PCR with reverse transcription and a reporter assay (left) were carried out following transfection. **(c)** Cell lysate and medium from KLotho- and KLothoΔss-overexpressing

cells were subjected to immunoblotting with antibody against klotho (left). 293T cells were transfected with TOP/FOP reporter, in the presence of medium from cells exogenously expressing vector, Wnt3a or KLotho as indicated (middle). 293T cells were transfected with ΔRIG-I and IL-6 reporter in the presence of medium from KLotho-overexpressing cells followed by reporter assay (right). **(d)** 293T cells were transfected with the constructs as indicated. Cells were then cultured in the presence of klotho antibody αKL for 12 h after transfection. Samples were collected and subjected to qPCR analysis. All the above data are represented as means + s.d. of three independent experiments. * $P < 0.05$, ** $P < 0.01$.

Klotho blocks RIG-I multimerization

Klotho did not alter TRIF, MyD88 or MAVS signalling (Fig. 4a), indicating that inhibition of RIG-I signalling occurs through direct interaction with RIG-I. To test this possibility, we made several deletion forms of klotho. KLotho and KLothoΔss suppressed ΔRIG-I-induced activation of NF-κB, in a similar way to KLotho (Fig. 6a). KLotho also suppressed the activation of the IL-6 promoter by ΔRIG-I, whereas the carboxy terminus of KLotho did not, indicating that the KL1 domain of klotho is essential for the suppression of NF-κB, IL-6 and IL-8 (Fig. 6a and Supplementary Fig S1c). We next tested whether klotho directly interacts with RIG-I. As shown in Fig. 6b, ectopic klotho and RIG-I interact when co-expressed in the cell. This interaction was confirmed by co-immunoprecipitation, showing that endogenous RIG-I and klotho could interact (Fig. 6c). To map the interacting region of klotho, several klotho fragments were constructed. We found that amino acids 34–365 are responsible for the suppression of pro-inflammatory cytokines. Co-immunoprecipitation confirmed that amino acids 34–365 of klotho are important for the interaction with RIG-I and these data also demonstrated that the CARD of RIG-I mediates interaction with klotho (Fig. 6b).

Activation of RIG-I requires the multimerization of the CARD domain, and therefore we further tested whether klotho inhibits

this multimerization. RIG-I was overexpressed with KLotho or the amino-acid 34–293 fragment. The multimerization was analysed by native polyacrylamide gel electrophoresis followed by immunoblotting using an antibody against RIG-I. Multimerization of RIG-I was almost completely blocked in the presence of KLotho, and not by fragment 34–293 (Fig. 6d). We also show in Fig. 6e that endogenous RIG-I multimer was observed in senescent, but not in pre-senescent, HUVECs, and overexpression of klotho led to the inhibition of multimer formation. The results indicate that the binding of klotho to RIG-I inhibits the multimerization of RIG-I and thus blocks its signalling to drive the expression of inflammatory factors.

DISCUSSION

Senescence-associated inflammation was initially recognized by gene profiling experiments⁶. It is also known that inflammatory factors such as IL-6 and IL-8 promote the progression of senescence^{4,7}. However, the underlying mechanisms of senescence-associated inflammation are largely unknown. Klotho is an anti-ageing factor with many functions, but a role in age-related inflammation has not yet been explored. Various studies have demonstrated that both replicative senescence and oncogene-induced senescence mimic

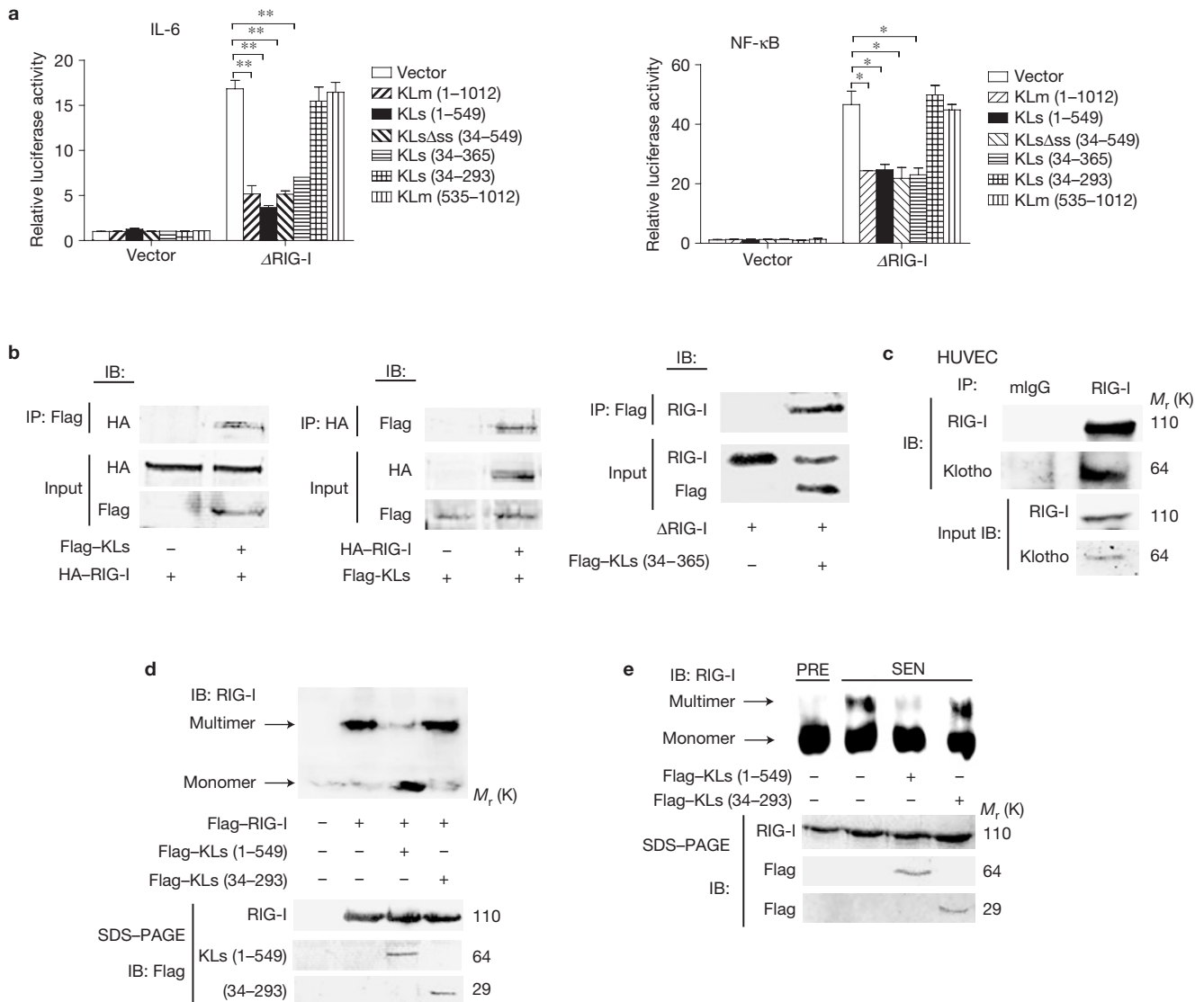


Figure 6 Inhibition of RIG-I-mediated expression of interleukins by Klotho through the block of RIG-I multimerization. **(a)** The inhibitory region of Klotho lies in the N terminus of the KL1 domain. 293T cells were transfected with different KLotho constructs and indicated reporter plasmids. Luciferase assay was carried out 24 h after transfection. Error bars represent means \pm s.d. ($n=3$). * $P < 0.05$, ** $P < 0.01$. **(b)** Klotho interacts with the RIG-I CARD domain. 293T cells were transfected as indicated. Total cellular protein was immunoprecipitated with anti-haemagglutinin (HA) or anti-Flag respectively. The precipitates were analysed by immunoblot assay with antibodies against the different tags. **(c)** Endogenous interactions of Klotho with RIG-I. Cell

lysate from pre-senescent HUVECs (10^8) was immunoprecipitated with mouse anti-RIG-I antibody or mouse IgG (mlgG). The immunoprecipitates and the expression levels of the endogenous proteins were analysed by immunoblots with antibodies against Klotho and RIG-I, respectively. **(d,e)** 293T cells (left) and HUVECs (right; PRE, pre-senescent; SEN, senescent) were transfected with the indicated expression plasmids for 24 h. Total protein was extracted and subjected to native polyacrylamide gel electrophoresis. The immunoblot analysis was carried out with an antibody against RIG-I. Ectopic gene expression was monitored by immunoblotting with an anti-Flag antibody following SDS-polyacrylamide gel electrophoresis.

the inflammatory responses in cells of multiple origins. Although initial studies have implicated CCAAT-enhancer-binding protein- β (C/EBP β) and NF- κ B as potential transcriptional activators of inflammatory cytokines in senescent cells, the upstream pathways responsible for the induction of these cytokines are unknown at present. RIG-I is expressed in the cytosol, and following ligation with dsRNA activates two distinct signalling pathways: IRF3 and NF- κ B. We show here that RIG-I expression is increased *in vitro* during cell passages (replicative senescence) as well as *in vivo* in various tissues of aged mice, and this age-related induction of RIG-I leads to increased basal expression of IL-6 and IL-8. We

also show that persistent activation of the DNA damage response induces RIG-I with IL-6, which depends on the activation of ATM. Senescence is tightly associated with the DNA damage response³⁴. An attractive explanation for increased inflammation during ageing is that DNA damage triggers inflammation through the induction of RIG-I and activation of its signalling. Replicative senescence also induced the expression of IRF1, a key transcription factor for the expression of RIG-I in senescent cells (Supplementary Fig. S2). Together with the literature, these data indicate that the IRF1-RIG-I axis mediates senescence-associated inflammation in an ATM-dependent manner.

It has been shown that RIG-I-induced IL-6 and IL-8 expression requires downstream signalling, and in particular the adaptor protein MAVS. Here, we show that MAVS-deficient MEFs show impaired senescence-associated inflammation, confirming a key role for RIG-I signalling in the increased levels of IL-6 observed during ageing. We further show that silencing of RIG-I and expression of *klotho* both slow the senescence process, which is consistent with the observations that inflammation promotes and maintains senescence. It should be noted that senescence-associated expression of IL-6 was not completely blocked in MAVS-deficient MEFs, indicating that other pathways are involved in age-related inflammation.

Induction and activation of RIG-I in senescent cells leads to the activation of NF- κ B, but not IRF3. It is known that RIG-I-mediated signalling bifurcates downstream of MAVS, so it is possible that downstream signalling molecules that activate IRF3 might be inactivated during senescence process. Future studies into the role of downstream molecules such as TRAFs, FADD and RIP1 could help us to understand the underlying mechanisms.

Two forms of *klotho* have been described¹³, a membrane form and a secreted form. It has also been proposed that the transcript for the secreted form of *klotho* is dominant in humans, whereas the membrane form of *klotho* is dominant in mice^{13,14}. We confirmed the presence of the secreted form of *klotho* (relative molecular mass, M_r , 64,000 (64 K)) in human cells, and this protein was decreased in senescent cells, consistent with the decrease of mRNA. Interestingly, KLS did not affect RIG-I signalling, although it inhibited the Wnt pathway. Both the membrane and secreted forms (M_r 130 K for KLM and 64 K for KLS), and the intracellular form (KLS Δ ss), can suppress RIG-I-mediated expression of IL-6 and IL-8 through the interaction with RIG-I. Extracellularly, *klotho* functions as a ligand or a co-receptor through the interaction with membrane-bound receptors, whereas intracellularly *klotho* functions as an endogenous inhibitor to suppress RIG-I signalling by binding to its CARD domain.

Loss of *klotho* gives rise to ageing-like phenotypes, such as emphysema and osteoporosis⁹, which are all considered as chronic inflammatory diseases. Here we demonstrate that many tissues in *kl/kl* mice express and secrete more inflammatory factors, and accumulate more IL-6 in serum, compared with wild-type mice. Therefore, age-related syndromes in *klotho*-deficient mice may result from chronic inflammation. The upregulation of RIG-I and inflammatory factors such as IL-6 and IL-8 correlates with the downregulation of *klotho*, which may explain why basal and induced pro-inflammatory cytokine expression increases during ageing. Therefore, upregulation of *klotho* may inhibit senescence-associated inflammation, slow the senescence procession and prolong the life span.

RIG-I signalling mediates senescence-associated inflammation, which is suppressed by intracellular *klotho* both *in vitro* and *in vivo*. Therefore, in addition to the role as an extracellular or membrane-bound factor, *klotho* also functions as an intracellular inflammatory inhibitor and anti-senescence factor. □

METHODS

Methods and any associated references are available in the online version of the paper at <http://www.nature.com/naturecellbiology/>

Note: Supplementary Information is available on the Nature Cell Biology website

ACKNOWLEDGEMENTS

We thank H. Shu, C. R. Abraham, M. Kuro-o, R. T. Moon and Y. Yang for plasmids, H. Deng and Y. Gao for irradiation, J. Luo and T. Tong for cell lines, Z. J. Chen and M. Kuro-o for knockout mice, M. Kuro-o for comments and J. L. Teeling for revising this paper. This work was supported by grants (2010CB911801 and 2011CB503904) from the National Basic Research Program, China.

AUTHOR CONTRIBUTIONS

F.L. and S.W. designed and conducted experiments, analysed the data and wrote the manuscript. H.R. carried out experiments. J.G. designed experiments and analysed the data, and wrote the manuscript.

COMPETING FINANCIAL INTERESTS

The authors declare no competing financial interests.

Published online at <http://www.nature.com/naturecellbiology>

Reprints and permissions information is available online at <http://npg.nature.com/reprintsandpermissions/>

- Hayflick, L. & Moorhead, P. S. The serial cultivation of human diploid cell strains. *Exp. Cell Res.* **25**, 585–621 (1961).
- Serrano, M., Lin, A. W., McCurrach, M. E., Beach, D. & Lowe, S. W. Oncogenic *ras* provokes premature cell senescence associated with accumulation of p53 and p16INK4a. *Cell* **88**, 593–602 (1997).
- Wei, W., Hemmer, R. M. & Sedivy, J. M. Role of p14(ARF) in replicative and induced senescence of human fibroblasts. *Mol. Cell Biol.* **21**, 6748–6757 (2001).
- Kuilman, T. *et al.* Oncogene-induced senescence relayed by an interleukin-dependent inflammatory network. *Cell* **133**, 1019–1031 (2008).
- Coppe, J. P. *et al.* Senescence-associated secretory phenotypes reveal cell-nonautonomous functions of oncogenic RAS and the p53 tumor suppressor. *PLoS Biol.* **6**, 2853–2868 (2008).
- Shelton, D. N., Chang, E., Whittier, P. S., Choi, D. & Funk, W. D. Microarray analysis of replicative senescence. *Curr. Biol.* **9**, 939–945 (1999).
- Acosta, J. C. *et al.* Chemokine signaling via the CXCR2 receptor reinforces senescence. *Cell* **133**, 1006–1018 (2008).
- Sebastian, T., Malik, R., Thomas, S., Sage, J. & Johnson, P. F. C/EBP β cooperates with RB:E2F to implement Ras(V12)-induced cellular senescence. *EMBO J.* **24**, 3301–3312 (2005).
- Kuro-o, M. *et al.* Mutation of the mouse *klotho* gene leads to a syndrome resembling ageing. *Nature* **390**, 45–51 (1997).
- Nagai, T. *et al.* Cognition impairment in the genetic model of aging *klotho* gene mutant mice: a role of oxidative stress. *FASEB J.* **17**, 50–52 (2003).
- Nagai, R. *et al.* Endothelial dysfunction in the *klotho* mouse and downregulation of *klotho* gene expression in various animal models of vascular and metabolic diseases. *Cell. Mol. Life Sci.* **57**, 738–746 (2000).
- Saito, Y. *et al.* *Klotho* protein protects against endothelial dysfunction. *Biochem. Biophys. Res. Commun.* **248**, 324–329 (1998).
- Matsumura, Y. *et al.* Identification of the human *klotho* gene and its two transcripts encoding membrane and secreted *klotho* protein. *Biochem. Biophys. Res. Commun.* **242**, 626–630 (1998).
- Shiraki-lida, T. *et al.* Structure of the mouse *klotho* gene and its two transcripts encoding membrane and secreted protein. *FEBS Lett.* **424**, 6–10 (1998).
- Xiao, N. M., Zhang, Y. M., Zheng, Q. & Gu, J. *Klotho* is a serum factor related to human aging. *Chin. Med. J. (Engl)* **117**, 742–747 (2004).
- Tsujikawa, H., Kurotaki, Y., Fujimori, T., Fukuda, K. & Nabeshima, Y. *Klotho*, a gene related to a syndrome resembling human premature aging, functions in a negative regulatory circuit of vitamin D endocrine system. *Mol. Endocrinol.* **17**, 2393–2403 (2003).
- Kurosu, H. *et al.* Regulation of fibroblast growth factor-23 signaling by *klotho*. *J. Biol. Chem.* **281**, 6120–6123 (2006).
- Urakawa, I. *et al.* *Klotho* converts canonical FGF receptor into a specific receptor for FGF23. *Nature* **444**, 770–774 (2006).
- Chang, Q. *et al.* The β -glucuronidase *klotho* hydrolyzes and activates the TRPV5 channel. *Science* **310**, 490–493 (2005).
- Kurosu, H. *et al.* Suppression of aging in mice by the hormone *Klotho*. *Science* **309**, 1829–1833 (2005).
- Liu, H. *et al.* Augmented Wnt signaling in a mammalian model of accelerated aging. *Science* **317**, 803–806 (2007).
- Ikushima, M. *et al.* Anti-apoptotic and anti-senescence effects of *Klotho* on vascular endothelial cells. *Biochem. Biophys. Res. Commun.* **339**, 827–832 (2006).
- Mitobe, M. *et al.* Oxidative stress decreases *klotho* expression in a mouse kidney cell line. *Nephron Exp. Nephrol.* **101**, e67–e74 (2005).
- Yamamoto, M. *et al.* Regulation of oxidative stress by the anti-aging hormone *klotho*. *J. Biol. Chem.* **280**, 38029–38034 (2005).
- Yoneyama, M. *et al.* The RNA helicase RIG-I has an essential function in double-stranded RNA-induced innate antiviral responses. *Nat. Immunol.* **5**, 730–737 (2004).
- Kato, H. *et al.* Cell type-specific involvement of RIG-I in antiviral response. *Immunity* **23**, 19–28 (2005).

27. Xu, L. G. *et al.* VISA is an adaptor protein required for virus-triggered IFN- β signaling. *Mol. Cell.* **19**, 727–740 (2005).
28. Seth, R. B., Sun, L., Ea, C. K. & Chen, Z. J. Identification and characterization of MAVS, a mitochondrial antiviral signaling protein that activates NF- κ B and IRF 3. *Cell* **122**, 669–682 (2005).
29. Meylan, E. *et al.* Cardif is an adaptor protein in the RIG-I antiviral pathway and is targeted by hepatitis C virus. *Nature* **437**, 1167–1172 (2005).
30. Kawai, T. *et al.* IPS-1, an adaptor triggering RIG-I- and Mda5-mediated type I interferon induction. *Nat. Immunol.* **6**, 981–988 (2005).
31. Wang, J. *et al.* Retinoic acid-inducible gene-I mediates late phase induction of TNF- α by lipopolysaccharide. *J. Immunol.* **180**, 8011–8019 (2008).
32. Poeck, H. *et al.* Recognition of RNA virus by RIG-I results in activation of CARD9 and inflammasome signaling for interleukin 1 β production. *Nat. Immunol.* **11**, 63–69 (2010).
33. Kubota, K. *et al.* Retinoic acid-inducible gene-I is induced in gingival fibroblasts by lipopolysaccharide or poly IC: possible roles in interleukin-1 β , -6 and -8 expression. *Oral Microbiol. Immunol.* **21**, 399–406 (2006).
34. Rodier, F. *et al.* Persistent DNA damage signalling triggers senescence-associated inflammatory cytokine secretion. *Nat. Cell Biol.* **11**, 973–979 (2009).
35. Pamment, J., Ramsay, E., Kelleher, M., Dornan, D. & Ball, K. L. Regulation of the IRF-1 tumour modifier during the response to genotoxic stress involves an ATM-dependent signalling pathway. *Oncogene* **21**, 7776–7785 (2002).
36. Kawaguchi, S. *et al.* Retinoic acid-inducible gene-I is constitutively expressed and involved in IFN- γ -stimulated CXCL9-11 production in intestinal epithelial cells. *Immunol. Lett.* **123**, 9–13 (2009).
37. Imaizumi, T. *et al.* Retinoic acid-inducible gene-I (RIG-I) is induced by IFN- γ in human mesangial cells in culture: possible involvement of RIG-I in the inflammation in lupus nephritis. *Lupus* **19**, 830–836 (2010).
38. Imaizumi, T. *et al.* Tumor-necrosis factor- α induces retinoic acid-inducible gene-I in rheumatoid fibroblast-like synoviocytes. *Immunol. Lett.* **122**, 89–93 (2009).
39. Imaizumi, T. *et al.* Involvement of retinoic acid-inducible gene-I in inflammation of rheumatoid fibroblast-like synoviocytes. *Clin. Exp. Immunol.* **153**, 240–244 (2008).
40. Maekawa, Y. *et al.* Klotho suppresses TNF- α -induced expression of adhesion molecules in the endothelium and attenuates NF- κ B activation. *Endocrine* **35**, 341–346 (2009).
41. Chen, C. D., Podvin, S., Gillespie, E., Leeman, S. E. & Abraham, C. R. Insulin stimulates the cleavage and release of the extracellular domain of Klotho by ADAM10 and ADAM17. *Proc. Natl Acad. Sci. USA* **104**, 19796–19801 (2007).

METHODS

Antibodies and plasmids. Goat anti-klotho (T-19) polyclonal antibody, rabbit anti- β -actin (I-19) polyclonal antibody, rabbit anti-IRF1 (C-20) polyclonal antibody, rabbit anti-goat IgG-AP, goat anti-mouse IgG-AP and goat anti-rabbit IgG-AP antibodies were from Santa Cruz Biotechnology. Rabbit anti-IRF3 (N-term) and anti-phospho-IRF3 (pS386) monoclonal antibodies were from Epitomics. Mouse anti-RIG-I (Alme-1) monoclonal antibody was from ALEXIS Biochemicals. Mouse anti-Flag monoclonal antibody and mouse anti-HA monoclonal antibody were from Sigma. All of the primary antibodies except anti-klotho (T-19) were diluted 1:10,000 and the secondary antibodies were diluted 1:20,000 for western blot. The Anti-klotho (T-19) was diluted 1:1,000 for western blot and 1:80 for the block experiment shown in Fig. 5d. NF- κ B, simian virus 40 (SV40), luciferase reporter plasmids and expression plasmid of RIG-I were provided by H. Shu (Wuhan University, Wuhan). The expression plasmids of the membrane form of human klotho and mouse klotho were from C. R. Abraham (Boston University School of Medicine, Boston) and M. Kuro-o (University of Texas Southwestern Medical Center, Dallas), respectively. TOPFlash, FOPFlash luciferase reporter plasmids and the expression plasmid of Wnt3a were gifts from R. T. Moon (University of Washington School of Medicine, Seattle) and Y. Yang (NIH, Bethesda). RNAi plasmids *GFP* shRNA and *ATM* shRNA were gifts from J. Campsi (Lawrence Berkeley National Laboratory, Berkeley). RIG-I-related promoter luciferase reporter plasmids, pSUPER-RIG-I RNAi plasmid, the secreted form of klotho and Δ RIG-I (amino acids 1–228) were generated in our laboratory.

Animals. Specific-pathogen-free KM mice were maintained *ad libitum* on a standard diet for either 6 (young mice) or 60 (old mice) weeks. Six mice (three males and three females) per group were used in the study. MAVS knockout (*mavs*^{-/-}) mice and klotho-deficient (*kl/kl*) mice were gifts from Z. Chen and M. Kuro-o (University of Texas Southwestern Medical Center, Dallas). Procedures involving animals and their care were approved by Peking University, which complies with the standards of Beijing Association on Laboratory Animal Care.

Mouse peritoneal macrophages were obtained according to a standard procedure reported previously³¹. To obtain RNA, 50 mg of each sample of tissues was homogenized with 1 ml TRNzol total RNA reagent (Tiangen).

Quantitative PCR with reverse transcription. Total RNA was isolated from mouse tissues, peritoneal macrophages or cultured cells using TRNzol total RNA reagent (Tiangen). One microgram of RNA was reverse transcribed using SuperScript III reverse transcriptase (Invitrogen) to generate first-strand complementary DNA, before subjecting the samples to quantitative PCR with specific primers (Supplementary Table S1).

Cell culture. HUVECs that underwent two population doublings were provided by J. Luo (Peking University, Beijing) and cells were maintained in M199 (HyClone), supplemented with 20% fetal bovine serum (FBS; Gibco), 5 ng ml⁻¹ human aFGF (Sigma) and 80 μ g ml⁻¹ heparin sodium (AppliChem) at 37 °C in a 5% CO₂ incubator.

MEFs were separated according to the *Stem Cell Culture Method Manual* (Invitrogen). Briefly, a female mouse at 13–14 days gestation was sacrificed and embryos removed from the uterine horn, by three washes of PBS. Embryos were placed in a fresh dish and washed three times to separate visceral tissue. Each head was used for genotype identification. Embryo tissue was minced using dissecting scissors, and 2 ml trypsin was added for 30 min incubation at 37 °C. Minced tissue was vigorously mixed with a pipette, and digestion was stopped by adding 2 ml DMEM for MEF (with 10% FBS and 10% non-essential amino acids (Invitrogen)). The mixture was then transferred to a 10 cm cell-culture dish with 10 ml DMEM for MEF, at 37 °C, and incubated for 4 h, before removing supernatants and replacing preheated DMEM for MEF. Only MEFs with a specified genotype (results from the head genotype identification) were used for relative experiments.

When the culture was confluent, cells were passaged by trypsinization and the cell number was counted. The added number of population doublings during each passage was calculated by the equation $A = \log_2 H - \log_2 S$ (A , added population doublings; H , collected cell number at the end of each passage; S , seeded cell number at the beginning of each passage).

WI-38 cells were provided by T. Tong (Peking University, Beijing). 293T and WI-38 cells were cultured in DMEM (HyClone), supplemented with 10% FBS (Gibco) at 37 °C in a 5% CO₂ incubator.

Senescence-associated β -gal staining. Senescence-associated β -gal activity of HUVECs and WI-38 was measured by a standard protocol described previously⁴².

Construction of RIG-I promoter reporter plasmids and klotho truncated mutants. Human genomic DNA was extracted from human primary HUVECs and

used as a template to clone the RIG-I promoter by PCR. The resulting sequence (–930 to –1 bp) was cloned into the XhoI and HindIII sites of pGL3-basic vector (Promega) to generate pGL3-1kb. Site-directed mutagenesis of the ISRE and IRF were introduced using the technique of PCR 'SOEING' with the mutagenic primers (mutations underlined): sense 5'-CAA TTA GAA ACC CCC CAT CTC ACG CCA CAA CA-3' and antisense 5'-AGA TGG GGG GTT TCT AAT TGT TTC AGC ACC GTT GT-3' were used for ISRE deletion, and sense 5'-CTC GAG ACA AAC GGT GCT GAA ACA AT-3' and antisense 5'-AAG CTT AAA GGG AAA GTC GTT AGT GC-3' were used for IRF mutation. For double mutation, sense 5'-CTC GAG ACA AAC GGT GCT GAA ACA AT-3' and antisense 5'-AAG CTT AAA GGG AAA GTC GTT AGT GC-3' were used. All of the mutations were identified by sequencing.

The full-length complementary DNA of the human secreted form of klotho was amplified by *TaKaRa LA Taq* using specific primers from total cDNA of human kidney. The PCR was subcloned into BamHI and XhoI sites of a Flag-tag vector modified from pcDNA3 vector (Invitrogen) in our laboratory. For truncated mutants, specific primers were used to amplify truncated klotho cDNA and subcloned into pGEM-T vector (Promega). The resulting plasmids were digested by BamHI and XhoI (NEB) and the fragments were cloned into the pcDNA3/Flag vector mentioned above.

Transfection and gene reporter assay. For transient transfections, 5×10^4 293T cells were seeded per well in a 24-well tissue-culture plate and cells were transfected 16 h later by the calcium phosphate precipitation procedure according to standard protocols. For HUVECs transfection, approximately 10^6 growing HUVECs were transfected with 0.4 μ g of SV40 and the reporter gene plasmid of interest (1:1), using jet PEI-HUVECs (Polyplus-transfection, Registre National des Brevets) following the manufacturer's instruction. HUVECs were washed with PBS and the culture medium was changed to fresh M199 with 20% FBS. After 24 h, cells were collected and a dual luciferase assay was carried out according to the manufacturer's instructions (Promega). For MEF transfection, approximately 10^6 growing MEFs were transfected with indicated plasmids using Lipofectamine 2,000 (Invitrogen) according to the manufacturer's instructions. After 24 h, cells and supernatants were collected for enzyme-linked immunosorbent assay (ELISA).

The dual luciferase reporter assay system (Promega) was used for luciferase assays. Cells were washed three times by PBS, and collected by passive lysis buffer (Promega), incubating for at least 15 min at room temperature. Dual luciferase assays were analysed according to the directions of the manufacturer (Promega).

Co-immunoprecipitation and western-blot analysis. Standard protocols have been reported previously⁴³. Briefly, after transfection with 10 μ g indicated plasmids for 24 h, 5×10^6 293T cells were washed with PBS and lysed in lysis buffer (20 mM Tris, pH 7.5, 150 mM NaCl, 1% Triton X-100, 1 mM EDTA, 10 μ g ml⁻¹ aprotinin, 10 μ g ml⁻¹ leupeptin, 1 mM phenylmethylsulphonyl fluoride). Young HUVECs (10^8) were used for endogenous co-immunoprecipitation assays. For immunoprecipitation, cell lysate was incubated with 1 μ g of the indicated antibody and 25 μ l of Protein A/G PLUS-Agarose (Santa Cruz Biotechnology) at 4 °C for about 4 h. The agarose beads were washed three times with 1 ml of lysis buffer after precipitation. The precipitates were analysed by standard immunoblot analysis with antibody as indicated.

Trichloroacetic acid precipitation. Proteins in culture medium were collected by this standard protocol described previously⁴¹.

Short interfering RNA information. For RIG-I, double-strand oligonucleotides corresponding to the target sequence of RIG-I cDNA were cloned into BglII and HindIII sites of pSUPER.retro.puro plasmid (OligoEngine). For *klotho*, *MAVS* and *IRF1*, short interfering RNA (siRNA) oligonucleotides targeting respective cDNA were designed and synthesized by GenePharma. All of the target sequences are listed in Supplementary Table S2.

ELISA. The supernatants of HUVECs and MEFs were collected after treatment as indicated. Human IL-6 level was measured by an ELISA kit from Boster. Mouse IL-6 level was measured by an ELISA kit from DAKWE.

Multimerization assay and electrophoretic mobility shift assay. Non-SDS-polyacrylamide gel (8%) was prerun with 25 mM Tris-HCl and 192 mM glycine, at pH 8.4, with and without 0.5% deoxycholate in the cathode and anode chamber for 30 min at 40 mA. Samples in the $\times 2$ native sample buffer (125 mM Tris-Cl, pH 6.8, 30% glycerol, 2% deoxycholate) were applied to the gel and electrophoresis carried out at 25 mA for 60 min. Immunoblot analysis was carried out with antibody as a standard procedure after electrophoresis. An electrophoretic

mobility shift assay (EMSA) was carried out by a standard protocol (Promega). The relative EMSA band intensity was quantified using Adobe Photoshop software, with reference to the negative control on the same film.

Viruses. Sendai virus was amplified and maintained in our laboratory. Lentiviruses encoding FG12 and FG12-siRIG-I have been described previously³¹.

Irradiation. Cells were X-ray-irradiated with total doses of 10 Gy at the rate of 1.2 Gy min⁻¹ (160 kV, 20 mA) using an RS2000 X-ray generator (RAD Source Technologies).

Statistical analysis. Statistical significance was determined by a two-tailed unpaired Student *t* test. * *P* < 0.05, ** *P* < 0.01, *** *P* < 0.001.

42. Dimri, G. P. *et al.* A biomarker that identifies senescent human cells in culture and in aging skin *in vivo*. *Proc. Natl Acad. Sci. USA* **92**, 9363–9367 (1995).
43. Xu, L., Xiao, N., Liu, F., Ren, H. & Gu, J. Inhibition of RIG-I and MDA5-dependent antiviral response by gC1qR at mitochondria. *Proc. Natl Acad. Sci. USA* **106**, 1530–1535 (2009).

Klotho suppresses RIG-I-mediated senescence-associated inflammation

Feng Liu, Su Wu, Hongwei Ren and Jun Gu

Nat. Cell Biol. **13**, 254–262 (2011); published online 20 February 2011; corrected after print 16 March 2011

In the version of this article initially published online and in print, the middle graph in Figure 3b was incorrectly labelled. Additionally two sentences on page 4 have been altered to; 'Interestingly, knockdown of RIG-I in senescent HUVECs led to extension of the lifespan of the senescent cells (Fig. 2g)...' and 'This is consistent with observations that inhibition of IL-6 and IL-8 extends the proliferative capacity of cultured cells passages^{4,5,7}..'. In the legend for figure 4c, wording has been changed to: '(c) Growth curves of control HUVECs and klotho-overexpressing HUVECs. Senescent HUVECs were transfected with control plasmid or klotho-expression plasmid'. On page 5, il-8 should have been IL-8. These errors have been corrected in both the HTML and PDF versions of the article.

DOI: 10.1038/ncb2167

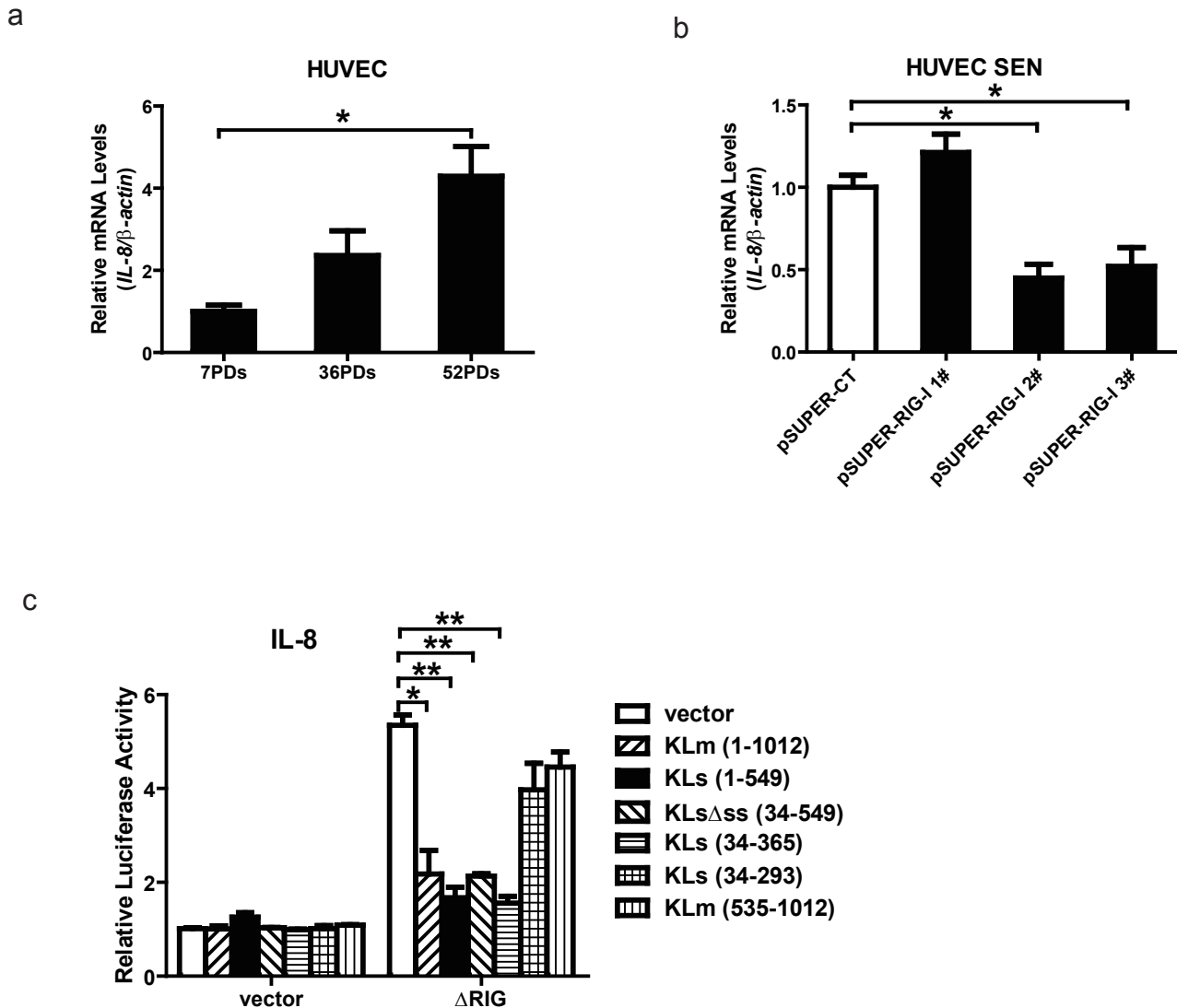


Figure S1 The effect of RIG-I and klotho on IL-8 expression in cell senescence. **(a)** Induction of IL-8 in HUVEC at indicated PDs. Total RNA was extracted and subjected to qPCR. Three independent cell populations in each passage were analyzed. Error bars represent mean + s.d. * $p < 0.05$ **(b)** Silence of RIG-I by interference plasmid in senescent HUVEC blocks the expression of IL-8. The same RIG-I interference plasmid was used

as mentioned in the methods. Total RNA was extracted and subjected to qPCR. **(c)** Inhibition of RIG-I activated IL-8 promoter by klotho. 293T were transfected with different klotho constructs and RIG-I CARD with IL-8 reporter plasmids, respectively. Luciferase assay were performed 24h after transfection. **(b)** and **(c)** error bars represent mean + s.d. (n=3) * $p < 0.05$. ** $p < 0.01$

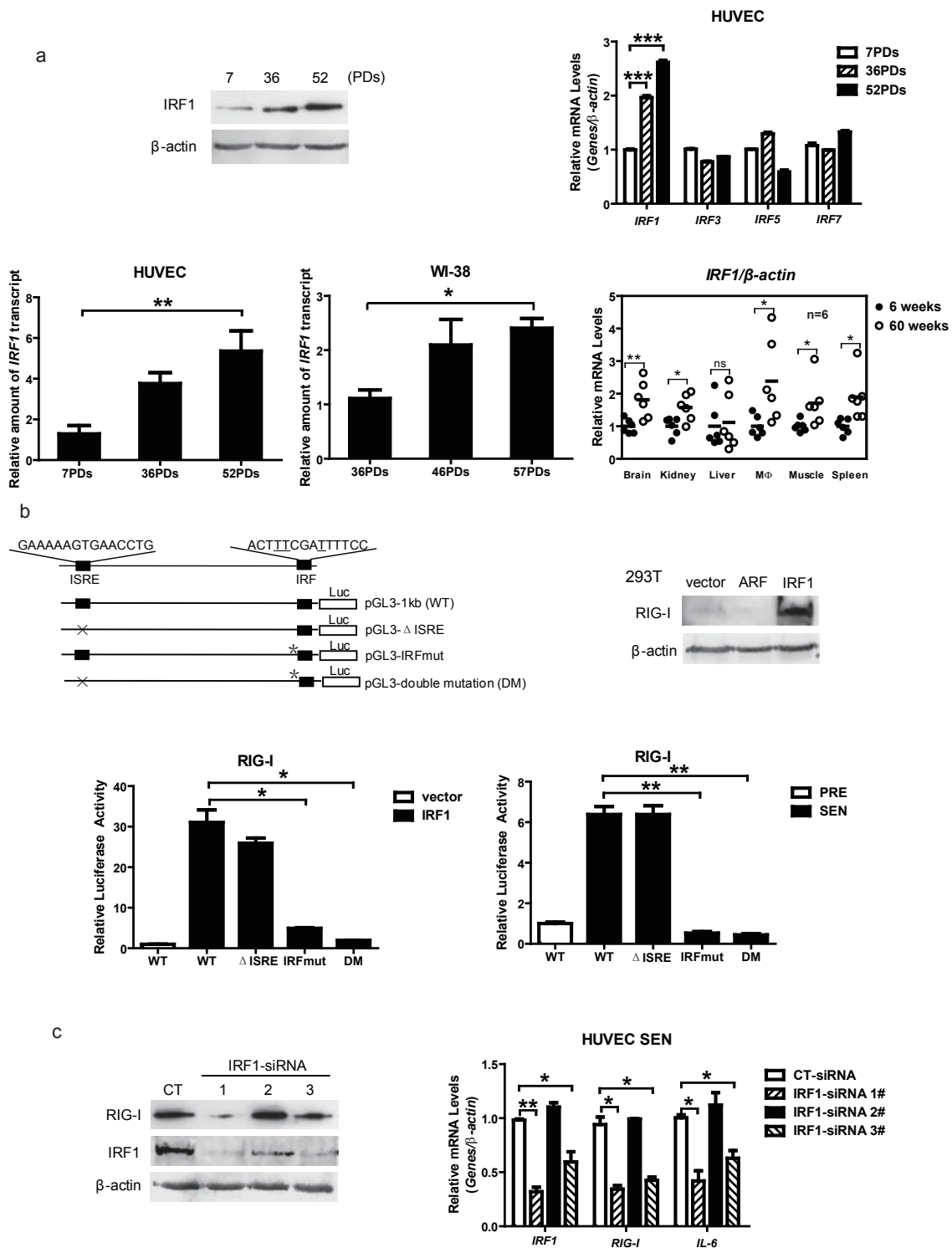


Figure S2 IRF1 involves in the replicative senescence associated inflammation through the induction of RIG-I. **(a)** Induction of IRF1 gene in *in vitro* and *in vivo* models. IRF1 was increased at mRNA and protein level at indicated PDs both in primary HUVEC and WI-38 cells, but IRF3/5/7 did not change much during cell replication. Three independent cell populations in each passage were analyzed. The up-regulation of IRF1 was also seen in different tissues of aged mice (60 week old). Six mice in each group were analyzed. Error bars represent mean + s.d. * $p < 0.05$. ** $p < 0.01$, *** $p < 0.001$. **(b)** IRF1 induces RIG-I at both transcriptional

and protein level. The construction of RIG-I promoters was described in the methods. Luciferase assay were performed 24h after transfection both in 293T cells and HUVEC (7PDs for presenescent cells and 52PDs for senescent cells). Three independent cell populations in each passage were analyzed. Error bars represent mean + s.d. (n=3) * $p < 0.05$. ** $p < 0.01$ **(c)** Silence of IRF1 by interference plasmids in senescent HUVEC blocks the expression of RIG-I and secretion of IL-6. Total RNA was extracted and subjected to qPCR. Error bars represent mean + s.d. (n=3) * $p < 0.05$. ** $p < 0.01$

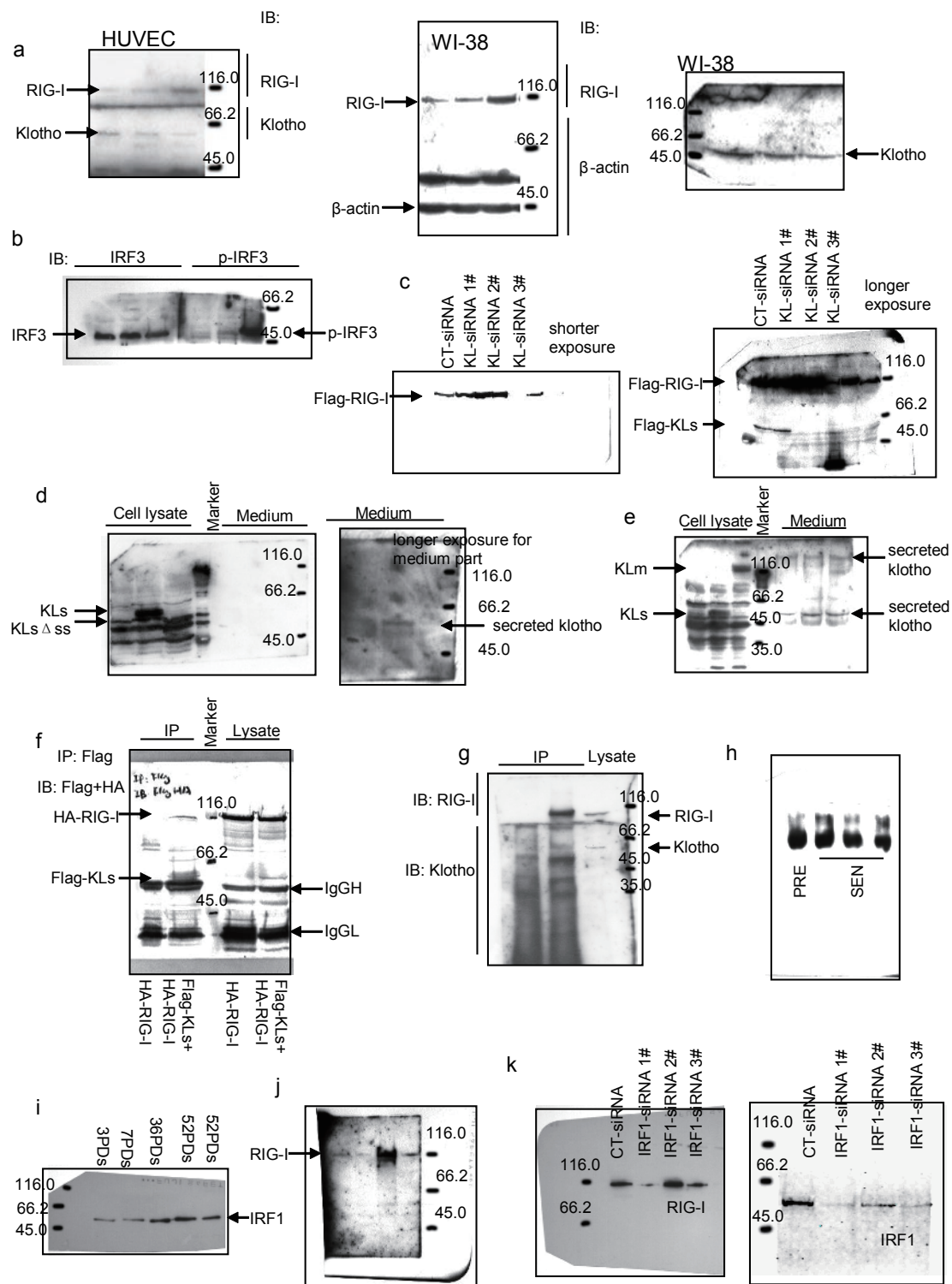


Figure S3 Supplementary full scans of western blots. (a) Full western for **Fig. 1c** verifying RIG-I and KL gene expression in HUVEC and WI-38 cells. (b) Full western for **Fig. 2e**, verifying IRF3 phosphorylation. (c) Full western for **Fig. 3a** verifying *klotho* gene depletion using RNAi (but not *rig-I*). (d) Full western for **Fig. 5a** verifying two forms of KL mutants. (e) Full western for **Fig. 5c** verifying secreted KL expression of either mutant form. (f) Full western for the first panel of **Fig. 6b** verifying Co-IP of HA-RIG-I by

Flag-KL. (g) Full western for **Fig. 6c** verifying endogenous Co-IP of RIG-I and KL. (h) Full western for **Fig. 6e** verifying KL blocks endogenous RIG-I multimer formation in senescent HUVEC. (i) Full western for **Fig. S1a** verifying IRF1 gene expression. (j) Full western for **Fig. S1b** verifying RIG-I gene expression induced by IRF1. (k) Full western for **Fig. S1c** verifying IRF1 gene depletion using RNAi, and accompanied by RIG-I expression change.

Table S1 Primers

| Genes | Primer pairs |
|----------------------|------------------------|
| Human IL-6 | TGACCCAACCACAAATGC |
| | CTGGCTCTGAAACAAAGGAT |
| Human IL-8 | TGTGGGTCTGTTGTAGGG |
| | GTGAGGTAAGATGGTGGC |
| Human RIG-I | GCATATTGACTGGACGTGGCA |
| | CAGTCATGGCTGCAGTTCTGTC |
| Human Klotho | TCAGGCAAGATAAACCAA |
| | TCTAACAAACGGGAACG |
| Human MDA5 | TTGTTATCCGTTATGGTCT |
| | TAGTGATGGGTTATTCTTGT |
| Human MAVS | AGTGAAAGGCACAAGGGAG |
| | CGTCTGATTGCGAGGAAA |
| Human β -actin | GTGGACATCCGCAAAGAC |
| | AAAGGGTGTAACGCAACTAA |
| Human IFN- β | CACTGGCTGGAATGAGACT |
| | TTTCGGAGGTAACCTGTAAG |
| Human IRF1 | GGCTGAAGCACAAGAATC |
| | AGTGCCTACTGTATTGAACG |
| Human IRF3 | AAAGAAGGGTTGCGTTTAGC |
| | TCAGGGACATGCCAGGGT |
| Human IRF5 | TGCGGACTGATGTGGAGA |
| | GGACAGGGAGATGAGGAAG |
| Human IRF7 | GGCAGATCCAGTCCCAACC |
| | GCAGCAGTTCCTCCGTGTAG |
| Mouse p16INK4a | CCCAACGCCCCGA ACT |
| | GCAGAAGAGCTGCTACGTGAA |
| Mouse RIG-I | GGCATTTCCTGTTTCTT |
| | GGTGGGCTTGGGATAGTC |
| Mouse Klotho | CCCAAACCATCTATGAAAC |
| | CTACCGTATTCTATGCCTTC |
| Mouse IL-6 | GGAAATCGTGGAATGAG |
| | GCTTAGGCATAACGCACT |
| Mouse GRO- α | ATGGCTGGGATTCACCTC |
| | TCGCACAACACCCTTCTA |
| Mouse β -actin | CACTGTGCCCATCTACGA |
| | CAGGATTCCATACCCAAG |
| Mouse IRF1 | GGGACATTGGGATAGGCA |
| | CTCAGGAGGGCAAGAACG |

Table S2 siRNA targeted sequences

| Name | Sequences |
|-----------------|---------------------------|
| pSUPER-RIG-I 1# | AACCAGAATTATCCCAACCGA |
| pSUPER-RIG-I 2# | AAAGTGGAAATCACGGATTAGC |
| pSUPER-RIG-I 3# | AATCTTGTCATCCTTTATGAG |
| CT-siRNA | UUCUCCGAACGUGUCACGUTT |
| KL-siRNA-1# | CCGUAUUUAUUGAUGGUGATT |
| KL-siRNA-2# | CCGAGAGCAUGAAGAAUAATT |
| KL-siRNA-3# | GGAUUGACCUUGAAUUUAATT |
| MAVS-siRNA-1# | GGCUGGGUGGAGUACUUCATT |
| MAVS-siRNA-2# | CCACCUUGAUGCCUGUGAATT |
| MAVS-siRNA-3# | CAGAGGAGAAUGAGUAUAAT T |
| IRF1-siRNA-1# | GCAGAUUAAUCCAACCAATT |
| IRF1-siRNA-2# | GCCGAGAUGC UAAGAGCAATT |
| IRF1-siRNA-3# | GCACCAGUGAUCUGUACAATT |